Kidins220/ARMS regulates Rac1-dependent neurite outgrowth by direct interaction with the RhoGEF Trio.

Veronika E Neubrand, Claire Thomas, Susanne Schmidt, Anne Debant, Giampietro Schiavo

Kidins220/ARMS regulates Rac1 dependent neurite outgrowth via a direct interaction with the RhoGEF Trio

Veronika E. Neubrand[1,3,‡], Claire Thomas[1], Susanne Schmidt[2], Anne Debant[2] and Giampietro Schiavo[1,‡]

[1]Molecular NeuroPathobiology, Cancer Research UK London Research Institute, 44 Lincoln's Inn Fields, London, WC2A 3PX, UK

[2]CRBM-CNRS, UMR5237, 1919 Route de Mende, 34293 Montpellier Cédex 05, France

[‡]To whom correspondence should be addressed:

Phone: +44 20 7269 3300/ +34 958 181621

Fax: +44 20 7269 3417/ +34 958 181632

e-mail: Giampietro.Schiavo@cancer.org.uk / vneubrand@ipb.csic.es

[3]present address: Instituto de Parasitologia y Biomedicina "Lopez-Neyra", Avda. Conocimiento S/N, Parque Tecnologico Ciencias de la Salud, 18100 Armilla – Granada, Spain

Running title: Kidins220/ARMS binds Trio

Words: 7,964

Summary

Neurite extension depends on extracellular signals leading to changes in gene expression and rearrangements of the actin cytoskeleton. A factor, that might be able to orchestrate these signalling pathways with cytoskeletal elements, is the integral membrane protein Kidins220/ARMS, a downstream target of neurotrophins. As its novel binding partner we identified Trio, a RhoGEF for Rac1, RhoG and RhoA, which is involved in neurite outgrowth and axon guidance. This interaction is direct and occurs between the N-terminus of Trio and the ankyrin repeats of Kidins220. Trio and Kidins220 co-localise at the tips of neurites in NGF-differentiated PC12 cells, where F-actin and Rac1 also accumulate. Expression of the ankyrin repeats of Kidins220 in PC12 cells inhibits NGF-dependent and Trio-induced neurite outgrowth. Similar results are seen in primary hippocampal neurons. Our data indicate that Kidins220 might localise Trio to specific membrane sites and regulate its activity, leading to Rac1 activation and neurite outgrowth.

Key words: neuronal differentiation, neurotrophin signalling, Kidins220/ARMS, Rac1, Trio

Introduction

During neuronal development, axons and dendrites have to navigate long distances to reach their physiological targets. This process includes extensive membrane remodelling and neurite elongation, which depend on extracellular signals that prompt changes in gene expression and cytoskeletal rearrangements at the growth cone. Amongst other extracellular inputs, neurotrophins play main roles in mediating neuronal differentiation, survival and death (Huber et al., 2003; Lu et al., 2005). Nerve growth factor (NGF), one of the best-characterised neurotrophins, signals through the neurotrophin receptors TrkA and $p75^{NTR}$. Upon NGF-binding, these receptors hetero-oligomerise and initiate pathways leading to sustained MAPK signalling, which is required for neurite outgrowth.

A molecule recently established to play a key role in sustained NGF-dependent MAPK signalling is Kidins220, also called ARMS (Arevalo et al., 2006; Arevalo et al., 2004; Hisata et al., 2007). Kidins220 is a highly conserved, integral membrane protein with large N- and C-terminal cytoplasmic domains (Iglesias et al., 2000; Kong et al., 2001). It acts as a downstream target of ephrin and neurotrophin receptors, such as $p75^{NTR}$ and TrkA (Arevalo et al., 2004; Kong et al., 2001), with which it forms a ternary complex (Chang et al., 2004). Overexpression of dominant-negative Kidins220 mutants (Arevalo et al., 2006; Bracale et al., 2007), or its downregulation by siRNA (Arevalo et al., 2004; Hisata et al., 2007) caused a strong inhibition of sustained MAPK signalling and neurite outgrowth in PC12 cells.

In addition to changes in gene expression, rearrangements of the actin cytoskeleton are essential for neurite elongation. Members of the small RhoGTPase family regulate this process, with Rac1, Cdc42 and RhoG supporting neurite extension and RhoA mediating growth cone retraction (Dickson, 2001; Govek et al., 2005). RhoGTPases cycle between

an active, GTP-bound form and an inactive, GDP-bound form. The activation is under the control of Rho guanine nucleotide exchange factors (RhoGEFs) specific for a subset of RhoGTPases (Rossman et al., 2005), whilst they are turned off by their corresponding RhoGTPase activating proteins (RhoGAPs).

Trio and its closely related family member Kalirin are recent additions to the growing family of RhoGEFs involved in neurite outgrowth. Both Trio and Kalirin possess two independent RhoGEF domains - the first one (GEF1) is specific for Rac1 and RhoG, and the second one (GEF2) for RhoA (Bateman and Van Vactor, 2001; Bellanger et al., 1998; Blangy et al., 2000; Debant et al., 1996; Penzes et al., 2001). Trio has been implicated in axon guidance in a variety of organisms, such as *C. elegans*, *D. melanogaster* and *M. musculus*, via its first GEF domain (Awasaki et al., 2000; Bateman et al., 2000; Briancon-Marjollet et al., 2008; Liebl et al., 2000; Lin and Greenberg, 2000; Newsome et al., 2000; Steven et al., 1998). Trio knockout mice die between embryonic day (E) 15.5 and birth (O'Brien et al., 2000). They display skeletal muscle deformity, aberrant cellular organisations in the brain (O'Brien et al., 2000) and axonal guidance defects, which relates to the involvement of Trio in netrin-1/DCC signalling (Briancon-Marjollet et al., 2008). Further studies showed that Trio also regulates the organisation of neuronal clusters in the hindbrain (Backer et al., 2007).

In PC12 cells Trio is the rate-limiting factor of NGF-induced neurite outgrowth by the activation of RhoG via GEF1 (Estrach et al., 2002). This process is regulated by the N-terminal spectrin domains of Trio and its first SH3 domain (Estrach et al., 2002). Whereas the effect of GEF1 of Trio on neurite outgrowth is easy to rationalise, the inhibition of NGF-induced neurite outgrowth observed by expressing the spectrin repeats and the first SH3 domain is still lacking a precise explanation.

To date, the mechanisms implicated in neurotrophin signalling down to the re-organisation of the actin cytoskeleton are only partially understood. Therefore factors capable of receiving and integrating extracellular signals, and at the same time, modulating the actin cytoskeleton, could play a key role in orchestrating signalling events and actin rearrangements leading to neurite outgrowth. Kidins220 is ideally placed to fulfil this function by acting as a scaffolding protein for neurotrophin-receptors (Arevalo et al., 2004; Kong et al., 2001) and providing docking sites for modulators of the actin cytoskeleton. In this manuscript, we show that the N-terminal ankyrin repeats of Kidins220 bind directly to the spectrin domains of the RhoGEF Trio. Overexpression of the ankyrin-rich domain of Kidins220 leads to an enhanced Rac1 activation and to an impairment of Trio- and NGF-induced neurite elongation. Altogether these data suggest that the interaction between Trio and Kidins220 plays an important role in neurite outgrowth in PC12 cells and primary neurons.

Results

Interaction between Kidins220 and Trio

To further explore the role of Kidins220 in neurite elongation, we searched for possible interacting partners by a yeast-two hybrid approach using the N-terminal domain of Kidins220 as bait. This intracellular domain consists of 11 ankyrin repeats (1-402aa) (Fig. 1A), but does not include the Walker A motif (467-474aa), which, together with the Walker B (771-775aa), forms a P-loop NTPase domain. The N-terminal 672aa of the RhoGEF Trio, containing the Sec14 and its first four spectrin domains (Fig. 1B), were among the positive hits (for a complete list of putative interactors see Table S1). This interaction was tested by re-transforming yeast either with the N-terminal domain of Kidins220 (1-402aa; Kidins220$^{1-402}$) or its C-terminus (1209-1762aa; Kidins220$^{1209-1762}$) together with Trio$^{1-672}$. Only yeast co-transformed with the ankyrin repeats of Kidins220 and the N-terminus of Trio showed robust growth (Fig. S1A), hence confirming this result of the yeast-two hybrid screen.

Next, we verified the interaction of Kidins220 with Trio by co-immunoprecipitation experiments of endogenous proteins in PC12 cells. Anti-Trio (Fig. 1C) and anti-Kidins220 antibodies (Fig. 1D) were able to specifically co-immunoprecipitate Kidins220 and Trio, respectively. This interaction was taking place both in the absence and in the presence of NGF (Fig. 1E), suggesting that the interaction of Trio and Kidins220 is largely constitutive, as it was also observed for the ternary complex formation between Kidins220 and the neurotrophin receptors p75^{NTR} and TrkA (Chang et al., 2004). The efficiency of the Trio-Kidins220 co-immunoprecitation was comparable to other known interactors of Kidins220, such as p75^{NTR} (Chang et al., 2004) or kinesin-1 (Bracale et al., 2007).

Because of the high sequence similarity between Trio and its closely-related family members Kalirins, we decided to test if Kidins220 also interacts with Kalirins. Although we did not detect an interaction between endogenous Kidins220 and Kalirins in the yeast-two hybrid screen, Kalirin9 weakly co-immunoprecipitated with Kidins220 in PC12 cells transfected with HA-tagged Kidins220 (Fig. 1F). Interestingly this Kalirin isoform was previously shown to interact with $p75^{NTR}$ and activate RhoA (Harrington et al., 2008). Since we found Trio in the yeast-two hybrid screen and we were able to co-immunoprecipitate both endogenous Trio and Kidins220, we focussed our investigation on this specific interaction.

To map the determinants of the interaction of Trio with Kidins220, co-immunoprecipitation experiments were performed with the indicated GFP-tagged Trio constructs (Fig. 1B,G). PC12 cells were transfected, treated with NGF for 24 hours and extracts were immunoprecipitated with anti-Kidins220 antibodies. As shown in Fig. 1G, the fragment containing the spectrin repeats of Trio ($Trio^{1-1203}$) was immunoprecipitated, whilst the other domains of Trio, including the large C-terminus ($Trio^{1813-3038}$), were not. This association was specific, since it was not detected when this lysate was incubated with a rabbit pre-immune serum (pre-I) used as negative control. Because the band of GFP-tagged $Trio^{1579-1816}$ was running at a similar molecular weight as the immunoglobulin heavy chain, anti-Kidins220 antibodies and pre-immune serum coupled to protein G sepharose were loaded on the same gel (Fig. 1G and Fig. S1B). Comparison of these lanes shows that the contaminating bands, indicated by black and grey arrowheads, have slightly different mobility than GFP-tagged $Trio^{1579-1816}$.

In order to test if the interaction between Kidins220 and Trio was direct, the His_6-tagged N-terminal ankyrin-rich domain of Kidins220 was expressed and purified as described in Materials and Methods. This fragment was subsequently incubated with either GST

alone or the GST-tagged Sec14 domain (Trio$^{1-232}$), spectrin domains 1-4 (Trio$^{255-699}$) and 5-8 (Trio$^{696-1203}$) (Fig. S1C). Both spectrin clusters and to a lesser extent the Sec14 domain bound to Kidins220$^{1-402}$ (Fig. 1H), indicating that this interaction is direct and that the N-terminus of Trio, including all spectrin domains, participates in the formation of the Trio/Kidins220 complex.

Kidins220 and Trio co-localise at neurite tips

The binding of Kidins220 to Trio suggests that Kidins220 may affect actin cytoskeleton dynamics. If this were the case, Kidins220 should localise at least in part in regions enriched in actin microfilaments. To test this hypothesis, PC12 cells were differentiated for 3 days with NGF, then fixed and stained for F-actin using fluorescently-labelled phalloidin, and for endogenous Kidins220. As shown in Fig. 2A,B, F-actin and Kidins220 showed an extensive overlap at neurite tips (arrows). This enrichment of Kidins220 at neurite tips was not due to an accumulation of plasma membrane or cytoplasm at these sites, since Kidins220 and a membrane-bound version of mRFP (mRFP-CAAX; Fig. 2C) or soluble GFP (Fig. 2D) did not show the same cellular distribution (arrowheads). Interestingly, Trio also localises to actin-rich regions at growth cones (Estrach et al., 2002), a finding that prompted us to directly compare the localisation of Trio and Kidins220. Because anti-Trio antibodies do not recognise the endogenous protein in immunofluorescence, GFP-tagged full length Trio was expressed in NGF-differentiated PC12 cells, which were then immunostained for Kidins220. Both proteins could be detected at the tip of neurites (Fig. 2E,F), indicating that the interaction between Trio and Kidins220 may take place on extending neurites and growth cones.

What is the molecular function of the Kidins220/Trio complex? Since Kidins220 is an integral membrane protein and interacts directly with Trio, it may drive the recruitment of the latter, a mainly cytosolic protein, to specific membrane domains. To test this hypothesis, we overexpressed HA-tagged Kidins220 in PC12 cells and tested whether the cellular localisation of Trio is influenced by full length Kidins220. Due to the absence of suitable anti-Trio antibodies for immunofluorescence (see above) and the very low transfection efficiency of full length Trio, we used a truncated Trio construct containing all spectrin repeats, the first GEF and SH3 domain (Fig. 1B). This Trio fragment ($Trio^{1-1813}$) was shown to mimic full length Trio in promoting NGF-induced neurite outgrowth in PC12 cells (Estrach et al., 2002). Whilst GFP-tagged $Trio^{1-1813}$ is partially cytoplasmic as judged by immunofluorescence (Fig. 3A), co-expression of this fragment with full length Kidins220 determined its recruitment onto Kidins220-positive membrane-bound punctae (double positive structures = 50.3% ± 7.4) (Fig. 3B,C; arrows). This effect was not observed in cells co-expressing full length Kidins220 and GFP (double positive structures = 5.3% ± 1.2) (Fig. 3D, arrowheads). In contrast to full length Kidins220, expression of the membrane-anchored $Kidins220^{403-1762}$, which lacks the Trio-binding domain, was not able to localise $Trio^{1-1813}$ to the membrane (double positive structures = 8.7% ± 3.3) (Fig. 3E,F; arrowheads), indicating that full length Kidins220 might help in localising Trio to specific membrane domains and as a consequence, regulate its cellular activities.

$Kidins220^{1-402}$ activates Rac1 but not RhoG

To investigate the functional effects of a Trio-Kidins220 complex, we tested whether Kidins220 would activate downstream effectors of Trio. Since NGF-induced neurite outgrowth is mediated by its first GEF domain (Estrach et al., 2002), we looked at the

activation of Rac1 and RhoG, both of which can be activated by this domain. Full length Kidins220, the Trio-interacting ankyrin repeats (Kidins220$^{1-402}$) and the remaining C-terminal portion of Kidins220 (Kidins220$^{403-1762}$) were expressed as HA-tagged proteins in HEK293 cells (see Materials and Methods and Fig. S2A). Cell lysates were then examined for the amount of activated, GTP-bound Rac1 using a GST-pull down assay performed with the Cdc42/Rac1 interacting-binding (CRIB) domain of the Rac1 effector protein Pak1. Overexpression of Kidins220$^{1-402}$ and to a small but significant extent full length Kidins220 led to a reproducible activation of Rac1 (Fig. 4A,B), suggesting a possible regulation of the TrioGEF1 activity by Kidins220.

However, these experiments did not address whether the Rac1 activation by Kidins220 was direct or due to the activation of RhoG, which in turn could activate Rac1 via the DOCK180/ELMO complex (Katoh and Negishi, 2003). To test this, we performed a RhoG activation assay with the GST-tagged kinectin domain 1 (KID1) of the RhoG effector kinectin (Vignal et al., 2001), following a protocol similar to that described above for the Rac1 activation. For the detection of endogenous RhoG, we used a monoclonal anti-RhoG antibody, which does not cross-react with Rac1 (Meller et al., 2008). HEK293 cells were transfected with HA-tagged Kidins220 constructs, GFP as negative and TrioGEF1 as positive control (Fig. S2C). As expected, TrioGEF1 potently activated endogenous RhoG (Fig. 4C). However, transfection of full length Kidins220 or Kidins220$^{1-402}$ did not affect the levels of GTP-bound RhoG (Fig. 4C,D), indicating that Rac1 activation by Kidins220 is direct and not mediated by RhoG.

Since Kidins220 was able to activate Rac1, we assessed the subcellular localisation of both proteins in differentiated PC12 cells. A pool of Rac1 localised to neurite tips and the staining of Kidins220 and Rac1 overlapped in these areas (Fig. 4E, arrows). However, Kidins220 and Rac1 did not co-localise on all neurite protrusions (Fig. 4E,

arrowheads), reflecting the possibility that not all neurites undergo dynamic changes at any given time, and some of them might even undergo retraction. Consistently, Aoki *et al*. found that in NGF-differentiated PC12 cells Rac1 was transiently activated at the cell periphery and neurite tips, and that this event was required for neurite outgrowth (Aoki et al., 2004). Next, we transfected GFP-tagged Trio in PC12 cells, and after 3 days of differentiation with NGF, the localisation of endogenous Rac1 and Kidins220 was revealed by immunostaining. As shown in Fig. 4F, the three proteins co-localised at some neurite tips, sites where they may actively promote neurite extension. This localisation is specific for Trio-GFP, since GFP was not enriched at these sites (Fig. 4G, arrowhead).

The ankyrin repeats of Kidins220 inhibit NGF-induced neurite outgrowth

Given the importance of Rac1 and Trio in neurite outgrowth, we wondered whether overexpression of Kidins220 and its fragments would affect this process. We decided to pursue this strategy instead of Kidins220 downregulation by RNA interference, since the latter approach, which has been previously shown to inhibit neurite outgrowth in PC12 cells (Hisata et al., 2007), would only provide insights on the overall function of Kidins220, but would not allow us to distinguish between the role of its interaction with Trio or with other binding partners (Arevalo et al., 2006; Arevalo et al., 2004; Bracale et al., 2007; Hisata et al., 2007; Iglesias et al., 2000; Kong et al., 2001; Luo et al., 2005). Therefore, we analysed the extent of NGF-induced differentiation in PC12 cells after overexpression of Kidins220$^{1\text{-}402}$, Kidins220$^{403\text{-}1762}$ and the full length protein, whilst GFP was used as a negative control (Fig. S3A). Cells were treated for 3 days with NGF, fixed, and the neurite length of transfected cells was measured and compared to the size of their cell bodies. Cells bearing at least one neurite twice the length of their cell body

were scored as positive. Overexpression of the N-terminal fragment, but not of Kidins220$^{403-1762}$ or full length Kidins220, inhibited neurite outgrowth (Fig. 5A, S3A). As shown in Fig. S3B and C, the ankyrin-rich Kidins220$^{1-402}$ domain is less expressed than Kidins220$^{403-1762}$ or Kidins220$^{1-1762}$, indicating that its inhibitory effect on neurite outgrowth (20.7% ± 2.2 differentiated cells versus 69% ± 6.9 in the case of GFP transfected cells; Fig. 5A) is not due its massive overexpression.

Based on these results, we wondered on how overexpression of Kidins220$^{1-402}$, which was able to drive Rac1 activation (Fig. 4A), could at the same time inhibit neurite outgrowth. As seen by immunofluorescence, the ankyrin repeats were distributed evenly throughout the cell (Fig. S3A, inset). Therefore, an attractive possibility is that Rac1 activation by Kidins220$^{1-402}$ occurs ubiquitously in transfected cells, instead of at specific sites on the plasma membrane, which is a prerequisite for neurite formation (Aoki et al., 2004; da Silva and Dotti, 2002). In this light, Kidins220$^{1-402}$ overexpression would mimic the inhibitory effect on NGF-dependent neurite outgrowth induced by overexpression of a constitutively active Rac1 mutant (Aoki et al., 2004). To test this hypothesis, we used the Raichu construct Rac1/Rac1-C-terminus (CT) as a biosensor to monitor Rac1 activation in live cells. This probe monitors the balance of activity between GEFs and GAPs acting on Rac1 and was previously used to study the localisation of activated Rac1 in NGF-treated PC12 cells (Aoki et al., 2004). We co-transfected this biosensor together with HA-tagged Kidins220$^{1-402}$ or Kidins220$^{403-1762}$ in PC12 cells and examined the localisation of activated Rac1. To this end, the FRET ratio between the emission intensities of acceptor and donor was measured in living cells (see Material and methods for details). In cells co-transfected with Kidins220$^{1-402}$ we observed an activation of Rac1 throughout the cell (Fig. 5B, upper panel). In contrast, cells co-transfected with the C-terminus of Kidins220, which we used as a negative

control, showed lower levels of GTP-bound Rac1 that partially localised along the plasma membrane (Fig. 5B, lower panel, arrows). Aoki and colleagues devised an elegant way of measuring cell areas with a FRET ratio above a certain threshold, which allows testing whether a localised activation of Rac1 is required for neurite outgrowth (Aoki et al., 2004). They could use as a reference the same cell before NGF treatment, whereas in our experiments, which involve two cell populations transfected with different constructs, we had to empirically set a threshold ratio above which we could detect a difference in Rac1 activation (see Material and methods). We observed a significant difference in the cell area occupied by activated Rac1 in cells co-transfected with Kidins220$^{1-402}$ or Kidins220$^{403-1762}$ at a FRET ratio above 2.4 (Fig. 5C). This result correlates well with our biochemical data (Fig. 4A,B). Cells transfected only with Raichu Rac1/Rac1-CT displayed an intermediate value (data not shown). At present we are unable to assess whether this difference is due to an inhibitory effect of the C-terminus of Kidins220, or whether the transfection of the Raichu construct alone results in a higher basal activation of Rac1.

Taken together, these results suggest that the ankyrin repeats of Kidins220 triggered a ubiquitous activation of Rac1. Since a localised activation of Rac1 at specific sites at or close to the plasma membrane is necessary for neurite extension, overexpression of Kidins220$^{1-402}$ determined as a consequence a net inhibition in NGF-induced neurite outgrowth (Fig. 5A).

Effect of Kidins220 on Trio- and RhoG-induced neurite elongation

To study more specifically the functional consequences of the interaction between Kidins220 and Trio, we looked at the effect that Kidins220 and its deletion mutants might have on Trio-induced neurite outgrowth. To this end, PC12 E2 cells, a PC12 cell

clone with enhanced sensitivity to neurite outgrowth promoting factors (Estrach et al., 2002; Wu and Bradshaw, 1995), were double transfected with GFP-Trio$^{1-1813}$ and either mRFP, full length Kidins220 or its deletion mutants. As in Fig. 3, we used the C-terminal truncated version of Trio (Trio$^{1-1813}$), since this mutant induces neurite outgrowth in PC12 cells (Estrach et al., 2002), but its transfection efficiency is higher than full length Trio. After transfection, cells were incubated for 48 hours in full growth medium, then fixed and analysed for their neurite length as described above. Under these conditions, expression of full length Kidins220 alone induced a minor increase (9.2% ± 1.6) in neurite outgrowth, compared to 4.9% (± 1.2) in mRFP expressing cells ($p = 0.077$) and to 3.6% (± 0.9) in Kidins220$^{1-402}$ expressing cells ($p = 0.023$) (Fig. 6A). In co-transfection experiments, only double expressing cells were examined for neurite outgrowth as described before (Fig. S4). Cells double-transfected with Trio$^{1-1813}$ and mRFP showed neurite outgrowth in 35.3% (± 4.7) of cases, representing the baseline for Trio-induced neurite outgrowth (Fig. 6C; n=3 independent experiments). Expression of full length Kidins220 or Kidins220$^{403-1762}$ did not significantly alter Trio-induced neurite elongation, whilst expression of Kidins220$^{1-402}$ significantly inhibited this process (Fig. 6C). Since Kidins220$^{1-402}$ is partially cytosolic (Fig. 6F), we wondered whether a membrane-bound variant of Kidins220$^{1-402}$ would exert the same effect. Therefore we added a CAAX box at the C-terminus of Kidins$^{1-402}$, a modification that has previously shown to determine prenylation and recruitment of soluble proteins to the membrane. As shown in Fig. 6F, CAAX-tagged Kidins220$^{1-402}$ was bound to the membrane pellet. However, it was still able to reduce Trio-induced neurite outgrowth (Fig. 6D), indicating that this inhibitory effect is independent of the membrane association of Kidins$^{1-402}$ and is rather the result of its ubiquitous localisation (Fig. S5, inset).

As previously shown for Trio, its downstream target RhoG is also able to promote neurite elongation when overexpressed (Estrach et al., 2002; Katoh et al., 2000). Since Kidins220$^{1-402}$ led to the specific activation of Rac1 and not RhoG, we anticipated that overexpression of the ankyrin repeats should not affect the RhoG-induced neurite outgrowth. Therefore, PC12 E2 cells were double transfected with wild type RhoG-GFP together with either mRFP or Kidins220 deletion mutants for 48 hours (Fig. S6). Neither the N- nor C-terminal domains of Kidins220 altered neurite outgrowth induced by RhoG (Fig. 6E; n=3 independent experiments). These results confirm our biochemical evidence that the ankyrin repeats of Kidins220 did not promote RhoG activation. However, co-expression of full length Kidins220 with wild type RhoG doubled the number of cells bearing neurites (Fig. 6E), indicating that full length Kidins220 and RhoG might synergise with each other.

The N-terminus of Kidins220 inhibits neurite outgrowth in primary neurons

To confirm the role of the Trio-Kidins220 interaction in neurite elongation, we tested the effect of Kidins220$^{1-402}$ in primary neurons. For this experiment we chose hippocampal neurons, because Trio knockout mice displayed abnormal neural organisation in the hippocampus (O'Brien et al., 2000) and Kidins220 is highly expressed in this region of the brain (Kong et al., 2001; Wu et al., 2009). Therefore E18 hippocampal neurons were nucleofected with Kidins220 deletion mutants and GFP as negative control. After 1 day *in vitro*, neurons were fixed and examined for their neurite length (Fig. 7A-C). Under these conditions, GFP-expressing hippocampal neurons had a normal appearance, with the majority of cells showing one or more neurites (Fig. 7A,D). Neurons expressing Kidins220$^{403-1762}$ also showed neurites at this stage (Fig. 7C,D). However, neurons overexpressing Kidins220$^{1-402}$ were not able to develop

neurites (Fig. 7B,D). Because of their round appearance, we were concerned that these cells might be necrotic or apoptotic. Therefore we performed a co-staining with propidium iodide, which labels the nucleus of necrotic cells when added before fixation. In addition, nucleofected neurons were treated with an antibody specific for the activated form of caspase 3, an early apoptosis marker. These tests revealed that neurons expressing Kidins220$^{1-402}$ were not necrotic (Fig. 7Bb, green) or apoptotic (Fig. 7Bb, red). Unfortunately, we were not able to express full length Kidins220 in neurons, due to its propensity to aggregate upon overexpression. Since hippocampal neurons expressing Kidins220$^{1-402}$ mostly did not bear neurites after one day *in vitro*, it is likely that the ankyrin repeats affects neurite initiation, which is important for both dendritic and axonal growth. This is in accordance with previous studies, which showed that Kidins220 regulated dendritic branching in *vivo* (Wu et al., 2009), and modulated the development of both axons and dendrites (Higuero et al., 2009). In summary, this experiment demonstrates that the inhibitory activity of the ankyrin-rich domain of Kidins220 on neurite outgrowth occurs also in hippocampal neurons, strongly suggesting that the pathway elucidated in PC12 cells has general validity and controls differentiation in primary neurons.

Discussion

In this manuscript we analysed the interaction of the scaffolding molecule Kidins220 with the RhoGEF Trio and its functional consequences. Mapping of the interaction sites between these two proteins revealed that the N-terminal ankyrin-rich domain of Kidins220 (Kidins220$^{1-402}$) bound directly to the N-terminal spectrin repeats of Trio. Both proteins co-localised at the tips of neurites in NGF-differentiated PC12 cells, where F-actin and Rac1 also accumulated. Rac1, but not RhoG, was specifically activated by Kidins220$^{1-402}$ and, to a small extent, by the full length protein. Strikingly, overexpression of the ankyrin repeats of Kidins220 inhibited neurite outgrowth, whereas its C-terminus had no effect.

Because expression of Kidins220$^{1-402}$ specifically inhibited both NGF- and Trio-induced neurite outgrowth, and NGF-mediated outgrowth depends on Trio (Estrach et al., 2002), it is likely that the dominant-negative effect elicited by Kidins220$^{1-402}$ is due to its interaction with the spectrin-rich domain of Trio. Our results might therefore explain the observed inhibitory effect of the latter domain on NGF-dependent differentiation (Estrach et al., 2002). The inhibition of neurite outgrowth by Kidins220$^{1-402}$ is not a general effect since its overexpression did not affect neurite extension induced by RhoG (Fig. 6E). This is in accordance with our biochemical data that Kidins220 did not activate RhoG. Furthermore, full length Kidins220 increased RhoG-induced neurite outgrowth (Fig. 6E). Because both RhoG and Kidins220 can activate Rac1 independently from each other (Fig. 8A; pathway A and B), contribution from these two signalling cascades could occur in parallel and thus their effects on neurite outgrowth could be additive. In contrast, full length Kidins220 was not able to synergise with Trio in promoting neurite elongation (Fig. 6C), suggesting that they may act on the same pathway (Fig. 8A; pathway B), with Trio being rate-limiting.

We observed a selective activation of Rac1, but not of RhoG, by the ankyrin repeats of Kidins220. Given the direct interaction between Kidins220 and Trio that we report here, we propose that the activation of Rac1 is mediated by Trio. This selectivity for Rac1 is not unprecedented. In fact, DCC/Netrin-induced neurite outgrowth mainly uses the Trio-dependent Rac1 pathway and a dominant-negative form of RhoG did not interfere with this process (Briancon-Marjollet et al., 2008). In addition, Backer and colleagues reported that Trio controls the organisation of neuronal clusters in the hindbrain via Rac1 and not RhoG (Backer et al., 2007), although previous reports show that Rac1 can be activated by RhoG via the DOCK180/ELMO complex (Katoh and Negishi, 2003). Since the TrioGEF1 domain is able to activate both RhoG and Rac1 (Bellanger et al., 1998; Blangy et al., 2000; Chhatriwala et al., 2007), one attractive possibility is that the specific process determines whether RhoG or Rac1 is activated. It was previously reported that RhoG, but not Rac1, mediated the membrane association of Trio, since Trio alone was not able to do so (Skrownek et al., 2004). In our system Trio might be recruited to the membrane with the help of Kidins220 instead of RhoG, since Kidins220 is an integral membrane protein and its binding to Trio must occur at specific membrane sites. In this scenario, Rac1 could be activated by Trio without an activation of RhoG and its downstream targets, such as Cdc42 (Gauthier-Rouviere et al., 1998).

The finding that the expression of Kidins220$^{1-402}$ activated Rac1 and inhibited neurite outgrowth phenocopies the effects of expressing constitutively-active Rac1, which also leads to a reduction of neurite outgrowth in PC12 cells (Aoki et al., 2004). A possible explanation for this phenomenon is that Rac1 needs to be activated at specific sites, such as neurite tips, to sustain neurite extension (Aoki et al., 2004). However, Kidins220$^{1-402}$ is not localised at these sites, allowing a ubiquitous activation of Rac1 (Fig. 5B) and consequently a block of differentiation (Fig. 8B; left). Full length

Kidins220, which also activated Rac1 although to a very small extent, did not prevent neurite elongation, most likely because it is correctly localised to neurite tips similarly to endogenous Kidins220 (Fig. 8B; right).

The phenotypic differences observed by expressing full length Kidins220 and its ankyrin-rich domain do not only originate from their different cellular localisation, but also derive from the fact that Kidins220 consists of two functionally distinct N- and C-terminal domains (see Fig. 1A), whose cross-talk is probably essential to exert its function as a scaffolding protein. In contrast to the full length protein, Kidins220$^{1-402}$ is unable to receive any information from the C-terminal portion of Kidins220, which is known to play a key role in the binding to neurotrophin receptors and contains several protein-protein interaction domains (Fig. 1A) (Arevalo et al., 2006; Arevalo et al., 2004; Bracale et al., 2007; Hisata et al., 2007; Iglesias et al., 2000; Kong et al., 2001; Luo et al., 2005). Crucially, the C-terminal domain undergoes tyrosine phosphorylation upon neurotrophin stimulation, and this event is required for the recruitment of downstream effectors necessary for sustained MAPK signalling (Arevalo et al., 2006) (pathway C in Fig. 8A).

Kidins220 might also exert its function through other Trio-related proteins. This view is supported by preliminary data showing that the inhibition of neurite outgrowth mediated by Kidins220$^{1-402}$ overexpression is still observed in neurons derived from Trio knockout mice (data not shown) (O'Brien et al., 2000), and by the interaction between Kidins220 and Kalirin, a Trio family member. Altogether, these results suggest that the functions of Trio and Kalirin might overlap. This is not surprising, since in *C. elegans* only one member of the Trio/Kalirin family, called Unc-73, is expressed (Bateman and van Vactor, 2001), suggesting that multiple roles for Trio and Kalirin were acquired with the increased complexity of the organisms. Interestingly, Kidins220 interacts with

the TrkB receptor and is phosphorylated upon treatment with its ligand brain-derived neurotrophic factor (BDNF) (Arevalo et al., 2004; Kong et al., 2001; Luo et al., 2005). In addition, Kidins220 is a downstream target of ephrins (Kong et al., 2001; Luo et al., 2005), which similarly to TrkB control dendritic spine morphology (Ethell et al., 2001; Gorski et al., 2003; Horch and Katz, 2002; Horch et al., 1999; Klein, 2004; Penzes et al., 2003). Accordingly, Kidins220 is enriched at the postsynaptic density (Wu and Chao, personal communication), and dendritic spine stability is significantly reduced in Kidins220$^{-/+}$ mice (Wu et al., 2009). Interestingly it has been shown before that Kalirin plays a major role in dendritic spine morphogenesis (Cahill et al., 2009; Ma et al., 2003; Ma et al., 2008; Penzes et al., 2003; Penzes and Jones, 2008), suggesting a new connection by Kidins220 between these pathways.

In this light, the interaction of Kidins220 with Trio or other Trio/Kalirin family members is likely to be crucial to control neuronal differentiation and functions *in vivo*. The work presented here might describe a basic molecular mechanism underlying this process. Thus, the scaffolding protein Kidins220 possesses all the prerequisites to co-ordinate different input signals from neurotrophins and ephrins with cytoskeletal rearrangements controlled by Trio/Kalirin and Rac1.

Material and methods

Plasmids

GFP-tagged Trio and RhoG were previously described in Estrach et al. 2002, and the GST-tagged CRIB domain of Pak1 and the KID1 domain of kinectin in Briancon-Marjollet et al., 2008 and Vignal et al., 2001. The Raichu construct Rac1/Rac-CT containing the coding sequence of Rac1, Rac1 C-terminus and the CRIB domain of Pak1 flanked with GFP reporters was a gift of M. Matsuda (Aoki et al., 2004; Yoshizaki et al., 2003). This construct was cloned into the pCAGGS expression vector, provided by J. Miyazaki (Niwa et al., 1991).

Cell culture and transfection

PC12 cells or PC12 E2 cells (Wu and Bradshaw, 1995) were cultured in DMEM (Gibco) supplemented with 7.5% fetal bovine serum (FBS) and 7.5% horse serum (HS), or 5% FBS and 10% HS, respectively. HEK293 cells were cultured in DMEM, 10% FBS. Cells were transfected using Lipofectamine 2000 (Invitrogen) and when indicated, treated with 100 ng/ml NGF (Alomone) for 3 days in DMEM, 0.1% FBS, 0.1% HS. Since the expression of Kidins220$^{1\text{-}402}$ was very low, the quantity of DNA for each construct was optimised to achieve similar expression levels in the RhoGTPase activation assays (Fig. S2A).

Hippocampal neurons were prepared from E18 embryos. 200,000 cells were transfected using the Amaxa nucleofector Small Cell Number Kit according to manufacturer's instructions and plated on coverslips coated with poly-L-lysine and laminin (both from Sigma) in DMEM, 10% HS. Subsequently, the medium was changed to Neurobasal Medium (Gibco) with 2% B27 (Invitrogen). 10 minutes before fixation, neurons were treated with propidium iodide, fixed and immunostained as described above.

Cells were analysed for neurite outgrowth by dividing the length of their longest neurite by the diameter of their cell body using Image J (National Institutes of Health). If this ratio was higher than two, cells were scored as positive. For the quantification of the experiment in Fig. 3, 10 cells per condition were analysed for Kidins220$^{1-1762}$ and Kidins220$^{403-1762}$ co-transfected with GFP-tagged Trio$^{1-1813}$ and 6 cells were analysed for Kidins220$^{1-1762}$ and GFP double-expressing cells. In total, 320 Kidins220$^{1-1762}$ and 416 Kidins220$^{403-1762}$ puncta were counted and scored positive when they also contained Trio$^{1-1813}$. 310 Kidins220$^{1-1762}$ positive puncta were similarly analysed in GFP double transfected cells.

FRET analysis of Rac1 activation

The Raichu construct Rac1/Rac1 CT (Aoki et al., 2004) was co-transfected with HA-tagged Kidins220$^{1-402}$ or Kidins220$^{403-1762}$ into PC12 cells plated on grid glass bottom dishes (Ibidi). After 1 day, images were taken on an inverted Nikon Eclipse TE 2000-E microscope equipped with a Xenon lamp, an iXon^{EM} CCD camera (Andor Technology) using a 100x oil immersion DIC objective with 1.4 N.A. Filters (T455LP, CFP dichroic; 51017bs, CFP/YFP dichroic; 430/24X and 500/20X, excitation filters; 470/24M and 533/30M, emission filters) were from Chroma. Images were acquired with Metamorph Software (Universal Imaging) in imaging medium (DMEM without phenol red, folic acid and riboflavin, but supplemented with 7.5% FBS and 7.5% HS) at 37°C and 10% CO_2. Each cell was imaged in the CFP, FRET (CFP excitation/YFP emission) and YFP channel to calculate the FRET ratio (FRET/CFP). After imaging, cells were fixed and immunostained with an anti-HA antibody followed by an AlexaFluor647-conjugated secondary antibody to identify double-transfected cells on a Zeiss confocal microscope. Bleed through between channels was assessed by expressing γ-BAR-CFP and γ-BAR-

YFP (Neubrand et al., 2005), and acquiring images using the same settings as optimised for the Raichu construct (1x1 binning, 500 ms exposure time for the CFP and FRET channel, 250 ms for the YFP channel). The measured bleedthrough of the CFP into FRET channel was 47% (± 0.75) corresponding to the CFP emission spectra. Since the correction for the CFP bleedthrough in the FRET channel results in the FRET ratio minus a constant ((FRET/CFP) - 0.47), and in this experiment these two conditions were directly compared with each other, this correction was neglected. The bleedthrough of the YFP channel into the FRET channel was assessed as a constant value of 20% (± 0.45) for different expression levels, and the formula above was corrected to (FRET - 0.2YFP)/CFP. After background subtraction, images were analysed using this formula in Metamorph (Universal Imaging). Resulting images were used to evaluate the FRET efficiency. In addition, expression levels of the Raichu construct were assessed in the YFP channel in each cell. For quantification purposes, only cells with expression levels between 500 and 5,000 grey levels in a 16-bit image were considered. A ratio between 0 and 4 with a binning of 10 grey levels in an 8-bit image was applied to each cell. Since we were unable to detect a significant difference between treated and control cells by simply averaging the FRET ratio over the whole cell, we chose the following strategy similar to the one proposed by Aoki et al. 2004. The cell area, which was occupied by a certain FRET ratio, was expressed as a percentage of the whole cell. Subsequently, the sum of these percentages above a certain threshold ratio was used to compare cell populations co-transfected with the Raichu construct and Kidins220$^{1\text{-}402}$ or Kidins220$^{403\text{-}1762}$. At the FRET ratio of 2.4, the highest significant value between cells co-transfected with Kidins220$^{1\text{-}402}$ and Kidins220$^{403\text{-}1762}$ was reached, as assessed with the Student's t-test.

Acknowledgements

We thank B. Larijani for her support with the FRET experiments and B. Eickholt for advice. We thank M. Matsuda and J. Miyazaki for the Raichu Rac1/Rac1 C-terminus constructs, and S. Hooper and E. Sahai for the CAAX-mRFP plasmid. We are grateful to A. Nicol and D. Aubyn for help with light microscopy and Metamorph software. This work was supported by Cancer Research UK (VEN, CT, GS), Fritz-Thyssen-Stiftung (VEN), CNRS and ANR-07-NEURO-006-01 from the Agence Nationale de la Recherche (SS and AD).

References

Aoki, K., Nakamura, T. and Matsuda, M. (2004). Spatio-temporal regulation of Rac1 and Cdc42 activity during nerve growth factor-induced neurite outgrowth in PC12 cells. *J Biol Chem* **279**, 713-9.

Arevalo, J. C., Pereira, D. B., Yano, H., Teng, K. K. and Chao, M. V. (2006). Identification of a switch in neurotrophin signaling by selective tyrosine phosphorylation. *J Biol Chem* **281**, 1001-7.

Arevalo, J. C., Yano, H., Teng, K. K. and Chao, M. V. (2004). A unique pathway for sustained neurotrophin signaling through an ankyrin-rich membrane-spanning protein. *Embo J* **23**, 2358-68.

Awasaki, T., Saito, M., Sone, M., Suzuki, E., Sakai, R., Ito, K. and Hama, C. (2000). The Drosophila trio plays an essential role in patterning of axons by regulating their directional extension. *Neuron* **26**, 119-31.

Backer, S., Hidalgo-Sanchez, M., Offner, N., Portales-Casamar, E., Debant, A., Fort, P., Gauthier-Rouviere, C. and Bloch-Gallego, E. (2007). Trio controls the mature organization of neuronal clusters in the hindbrain. *J Neurosci* **27**, 10323-32.

Bateman, J., Shu, H. and Van Vactor, D. (2000). The guanine nucleotide exchange factor trio mediates axonal development in the Drosophila embryo. *Neuron* **26**, 93-106.

Bateman, J. and Van Vactor, D. (2001). The Trio family of guanine-nucleotide-exchange factors: regulators of axon guidance. *J Cell Sci* **114**, 1973-80.

Bellanger, J. M., Lazaro, J. B., Diriong, S., Fernandez, A., Lamb, N. and Debant, A. (1998). The two guanine nucleotide exchange factor domains of Trio link the Rac1 and the RhoA pathways in vivo. *Oncogene* **16**, 147-52.

Blangy, A., Vignal, E., Schmidt, S., Debant, A., Gauthier-Rouviere, C. and Fort, P. (2000). TrioGEF1 controls Rac- and Cdc42-dependent cell structures through the direct activation of rhoG. *J Cell Sci* **113 (Pt 4)**, 729-39.

Bracale, A., Cesca, F., Neubrand, V. E., Newsome, T. P., Way, M. and Schiavo, G. (2007). Kidins220/ARMS is transported by a kinesin-1-based mechanism **Briancon-Marjollet, A., Ghogha, A., Nawabi, H., Triki, I., Auziol, C., Fromont, S., Piche, C., Enslen, H., Chebli, K., Cloutier, J. F. et al.** (2008). Trio mediates netrin-1-induced Rac1 activation in axon outgrowth and guidance. *Mol Cell Biol* **28**, 2314-23.

likely to be involved in neuronal differentiation. *Mol Biol Cell* **18**, 142-52.

Cahill, M. E., Xie, Z., Day, M., Barbolina, M. V., Miller, C. A., Weiss, C., Radulovic, J., Sweatt, J. D., Disterhoft, J. F., Surmeier, D. J. et al. (2009). Kalirin regulates cortical spine morphogenesis and disease-related behavioral phenotypes. *Proc Natl Acad Sci U S A* **106**, 13058-63.

Chang, M. S., Arevalo, J. C. and Chao, M. V. (2004). Ternary complex with Trk, p75, and an ankyrin-rich membrane spanning protein. *J Neurosci Res* **78**, 186-92.

Chhatriwala, M. K., Betts, L., Worthylake, D. K. and Sondek, J. (2007). The DH and PH domains of Trio coordinately engage Rho GTPases for their efficient activation. *J Mol Biol* **368**, 1307-20.

da Silva, J. S. and Dotti, C. G. (2002). Breaking the neuronal sphere: regulation of the actin cytoskeleton in neuritogenesis. *Nat Rev Neurosci* **3**, 694-704.

Debant, A., Serra-Pages, C., Seipel, K., O'Brien, S., Tang, M., Park, S. H. and Streuli, M. (1996). The multidomain protein Trio binds the LAR transmembrane tyrosine phosphatase, contains a protein kinase domain, and has separate rac-specific and rho-specific guanine nucleotide exchange factor domains. *Proc Natl Acad Sci U S A* **93**, 5466-71.

Dickson, B. J. (2001). Rho GTPases in growth cone guidance. *Curr Opin Neurobiol* **11**, 103-10.

Estrach, S., Schmidt, S., Diriong, S., Penna, A., Blangy, A., Fort, P. and Debant, A. (2002). The Human Rho-GEF trio and its target GTPase RhoG are involved in the NGF pathway, leading to neurite outgrowth. *Curr Biol* **12**, 307-12.

Ethell, I. M., Irie, F., Kalo, M. S., Couchman, J. R., Pasquale, E. B. and Yamaguchi, Y. (2001). EphB/syndecan-2 signaling in dendritic spine morphogenesis. *Neuron* **31**, 1001-13.

Gauthier-Rouviere, C., Vignal, E., Meriane, M., Roux, P., Montcourier, P. and Fort, P. (1998). RhoG GTPase controls a pathway that independently activates Rac1 and Cdc42Hs. *Mol Biol Cell* **9**, 1379-94.

Gorski, J. A., Zeiler, S. R., Tamowski, S. and Jones, K. R. (2003). Brain-derived neurotrophic factor is required for the maintenance of cortical dendrites. *J Neurosci* **23**, 6856-65.

Govek, E. E., Newey, S. E. and Van Aelst, L. (2005). The role of the Rho GTPases in neuronal development. *Genes Dev* **19**, 1-49.

Harrington, A. W., Li, Q. M., Tep, C., Park, J. B., He, Z. and Yoon, S. O. (2008). The role of Kalirin9 in p75/nogo receptor-mediated RhoA activation in cerebellar granule neurons. *J Biol Chem* **283**, 24690-7.

Higuero, A. M., Sanchez-Ruiloba, L., Doglio, L. E., Portillo, F., Abad-Rodriguez, J., Dotti, C. G. and Iglesias, T. (2009). Kidins220/ARMS modulates the activity of microtubule-regulating proteins and controls neuronal polarity and development. *J Biol Chem* **285**, 1343-57.

Hisata, S., Sakisaka, T., Baba, T., Yamada, T., Aoki, K., Matsuda, M. and Takai, Y. (2007). Rap1-PDZ-GEF1 interacts with a neurotrophin receptor at late

endosomes, leading to sustained activation of Rap1 and ERK and neurite outgrowth. *J Cell Biol* **178**, 843-60.

Horch, H. W. and Katz, L. C. (2002). BDNF release from single cells elicits local dendritic growth in nearby neurons. *Nat Neurosci* **5**, 1177-84.

Horch, H. W., Kruttgen, A., Portbury, S. D. and Katz, L. C. (1999). Destabilization of cortical dendrites and spines by BDNF. *Neuron* **23**, 353-64.

Huber, A. B., Kolodkin, A. L., Ginty, D. D. and Cloutier, J. F. (2003). Signaling at the growth cone: ligand-receptor complexes and the control of axon growth and guidance. *Annu Rev Neurosci* **26**, 509-63.

Iglesias, T., Cabrera-Poch, N., Mitchell, M. P., Naven, T. J., Rozengurt, E. and Schiavo, G. (2000). Identification and cloning of Kidins220, a novel neuronal substrate of protein kinase D. *J Biol Chem* **275**, 40048-56.

Katoh, H. and Negishi, M. (2003). RhoG activates Rac1 by direct interaction with the Dock180-binding protein Elmo. *Nature* **424**, 461-4.

Katoh, H., Yasui, H., Yamaguchi, Y., Aoki, J., Fujita, H., Mori, K. and Negishi, M. (2000). Small GTPase RhoG is a key regulator for neurite outgrowth in PC12 cells. *Mol Cell Biol* **20**, 7378-87.

Klein, R. (2004). Eph/ephrin signaling in morphogenesis, neural development and plasticity. *Curr Opin Cell Biol* **16**, 580-9.

Kong, H., Boulter, J., Weber, J. L., Lai, C. and Chao, M. V. (2001). An evolutionarily conserved transmembrane protein that is a novel downstream target of neurotrophin and ephrin receptors. *J Neurosci* **21**, 176-85.

Liebl, E. C., Forsthoefel, D. J., Franco, L. S., Sample, S. H., Hess, J. E., Cowger, J. A., Chandler, M. P., Shupert, A. M. and Seeger, M. A. (2000). Dosage-

sensitive, reciprocal genetic interactions between the Abl tyrosine kinase and the putative GEF trio reveal trio's role in axon pathfinding. *Neuron* **26**, 107-18.

Lin, M. Z. and Greenberg, M. E. (2000). Orchestral maneuvers in the axon: trio and the control of axon guidance. *Cell* **101**, 239-42.

Lu, B., Pang, P. T. and Woo, N. H. (2005). The yin and yang of neurotrophin action. *Nat Rev Neurosci* **6**, 603-14.

Luo, S., Chen, Y., Lai, K. O., Arevalo, J. C., Froehner, S. C., Adams, M. E., Chao, M. V. and Ip, N. Y. (2005). {alpha}-Syntrophin regulates ARMS localization at the neuromuscular junction and enhances EphA4 signaling in an ARMS-dependent manner. *J Cell Biol* **169**, 813-24.

Ma, X. M., Huang, J., Wang, Y., Eipper, B. A. and Mains, R. E. (2003). Kalirin, a multifunctional Rho guanine nucleotide exchange factor, is necessary for maintenance of hippocampal pyramidal neuron dendrites and dendritic spines. *J Neurosci* **23**, 10593-603.

Ma, X. M., Kiraly, D. D., Gaier, E. D., Wang, Y., Kim, E. J., Levine, E. S., Eipper, B. A. and Mains, R. E. (2008). Kalirin-7 is required for synaptic structure and function. *J Neurosci* **28**, 12368-82.

Meller, J., Vidali, L. and Schwartz, M. A. (2008). Endogenous RhoG is dispensable for integrin-mediated cell spreading but contributes to Rac-independent migration. *J Cell Sci* **121**, 1981-9.

Neubrand, V. E., Will, R. D., Mobius, W., Poustka, A., Wiemann, S., Schu, P., Dotti, C. G., Pepperkok, R. and Simpson, J. C. (2005). Gamma-BAR, a novel AP-1-interacting protein involved in post-Golgi trafficking. *Embo J* **24**, 1122-33.

Newsome, T. P., Schmidt, S., Dietzl, G., Keleman, K., Asling, B., Debant, A. and Dickson, B. J. (2000). Trio combines with dock to regulate Pak activity during photoreceptor axon pathfinding in Drosophila. *Cell* **101**, 283-94.

Niwa, H., Yamamura, K. and Miyazaki, J. (1991). Efficient selection for high-expression transfectants with a novel eukaryotic vector. *Gene* **108**, 193-9.

O'Brien, S. P., Seipel, K., Medley, Q. G., Bronson, R., Segal, R. and Streuli, M. (2000). Skeletal muscle deformity and neuronal disorder in Trio exchange factor-deficient mouse embryos. *Proc Natl Acad Sci U S A* **97**, 12074-8.

Penzes, P., Beeser, A., Chernoff, J., Schiller, M. R., Eipper, B. A., Mains, R. E. and Huganir, R. L. (2003). Rapid induction of dendritic spine morphogenesis by trans-synaptic ephrinB-EphB receptor activation of the Rho-GEF kalirin. *Neuron* **37**, 263-74.

Penzes, P., Johnson, R. C., Kambampati, V., Mains, R. E. and Eipper, B. A. (2001). Distinct roles for the two Rho GDP/GTP exchange factor domains of kalirin in regulation of neurite growth and neuronal morphology. *J Neurosci* **21**, 8426-34.

Penzes, P. and Jones, K. A. (2008). Dendritic spine dynamics--a key role for kalirin-7. *Trends Neurosci* **31**, 419-27.

Rossman, K. L., Der, C. J. and Sondek, J. (2005). GEF means go: turning on RHO GTPases with guanine nucleotide-exchange factors. *Nat Rev Mol Cell Biol* **6**, 167-80.

Steven, R., Kubiseski, T. J., Zheng, H., Kulkarni, S., Mancillas, J., Ruiz Morales, A., Hogue, C. W., Pawson, T. and Culotti, J. (1998). UNC-73 activates the Rac GTPase and is required for cell and growth cone migrations in C. elegans. *Cell* **92**, 785-95.

Vignal, E., Blangy, A., Martin, M., Gauthier-Rouviere, C. and Fort, P. (2001). Kinectin is a key effector of RhoG microtubule-dependent cellular activity. *Mol Cell Biol* **21**, 8022-34.

Wu, S. H., Arevalo, J. C., Sarti, F., Tessarollo, L., Gan, W. B. and Chao, M. V. (2009). Ankyrin Repeat-rich Membrane Spanning/Kidins220 protein regulates dendritic branching and spine stability in vivo. *Dev Neurobiol* **69**, 547-57.

Wu, Y. Y. and Bradshaw, R. A. (1995). PC12-E2 cells: a stable variant with altered responses to growth factor stimulation. *J Cell Physiol* **164**, 522-32.

Yoshizaki, H., Ohba, Y., Kurokawa, K., Itoh, R. E., Nakamura, T., Mochizuki, N., Nagashima, K. and Matsuda, M. (2003). Activity of Rho-family GTPases during cell division as visualized with FRET-based probes. *J Cell Biol* **162**, 223-32.

Figure legends

Figure 1: Interaction between Kidins220 and Trio. (A) Kidins220 is an integral membrane protein containing four transmembrane domains (TMs) and large N- and C-termini exposed to the cytoplasm. At the N-terminus, primary sequence analysis predicts 11 ankyrin repeats (1-402aa) and a Walker A motif (467-474aa), which together with the Walker B motif (771-775aa) forms a P-loop NTPase domain. The C-terminus contains a proline-rich domain, a sterile alpha motif (SAM)-like domain and a PDZ binding motif. Kidins220 binds kinesin light chain via the kinesin-1 interacting motif (KIM). Several phosphorylation sites are also present (not shown). The Kidins220 fragments used in this study are underlined. **(B)** Trio is a 348 kDa protein, comprised of a putative Sec14-like domain, followed by eight spectrin repeats (255-1203aa), two Rho-GEF and SH3 domains, an immunoglobulin (Ig)-like domain and a kinase domain at the C-terminus. The Trio fragments used in this study are underlined. **(C)** and **(D)** The interaction between Kidins220 and Trio was confirmed by co-immunoprecipitation of both endogenous proteins. NGF-treated PC12 cell extracts were immunoprecipitated with anti-Trio **(C)** or anti-Kidins220 antibodies **(D)**. Western Blots were probed with anti-Kidins220 and anti-Trio antibodies, respectively. In both experiments, endogenous Kidins220 and Trio were recovered in the pellet. **(E)** The association of Trio and Kidins220 was not modulated by NGF. To test whether the Kidins220-Trio interaction was NGF-dependent, PC12 E2 cells - a PC12 cell clone with enhanced sensitivity to neurite outgrowth promoting factors (Estrach et al., 2002; Wu and Bradshaw, 1995) - were incubated either without or with NGF for 24 hours, lysed and then immunoprecipitated with anti-Trio antibodies. **(F)** PC12 cells were transfected with HA-Kidins220 and HA-ULK1 as negative control, and then immunoprecipitated with anti-HA antibodies. The Western Blot was analysed with anti-Kalirin antibodies, which

revealed a weak band of Kalirin9 in the Kidins220 lane, but not in control immunoprecipitations. **(G)** To map the binding domains of Trio, PC12 cells were transfected with GFP-Trio constructs and lysates were immunoprecipitated with anti-Kidins220 antibodies. Immunoglobulin contaminating bands of the anti-Kidins220 antibodies and of the pre-immune serum (Pre-I) are indicated with black and grey arrowheads, respectively. Only the spectrin domains of Trio ($Trio^{1-1203}$) were immunoprecipitated by Kidins220 antibodies. **(H)** The ankyrin repeats of Kidins220 and the N-terminal fragments of Trio ($Trio^{1-232}$, $Trio^{255-699}$, $Trio^{696-1203}$) were expressed as recombinant proteins and tested for direct binding. The ankyrin repeats ($Kidins220^{1-402}$) bound to a small extent to the Sec14 domain ($Trio^{1-232}$), but they interacted equally well with the first ($Trio^{255-699}$) and the second half of the spectrin domains ($Trio^{696-1203}$). SN = supernatant; B = beads.

Figure 2: Co-localisation of Kidins220 and Trio. (A) NGF-differentiated PC12 cells were stained with phalloidin (green) and Kidins220 (red). Both markers overlapped partially at the neurite tips (arrows). **(B)** High magnification view of a neurite tip. PC12 cells were transfected with a membrane-bound mRFP construct (mRFP-CAAX) **(C)** or soluble GFP **(D)**, differentiated with NGF and stained for endogenous Kidins220. Arrowheads indicate the different cellular distribution of these proteins. **(E)** PC12 cells were transfected with Trio-GFP (green), differentiated with NGF and then immunostained for endogenous Kidins220 (red). Both proteins co-localised partially at neurite tips (arrows). See a high magnification view in **(F)**. Scale bars = 5 μm.

Figure 3: Trio associates with Kidins220-positive membrane structures. (A) and **(B)** PC12 cells were transfected with GFP-tagged $Trio^{1-1813}$ and HA-tagged full length

Kidins220, differentiated for 3 days with NGF, fixed and analysed by immunofluorescence. GFP-tagged Trio$^{1-1813}$ is partially diffused **(A)**, but it is recruited to Kidins220-positive punctae upon co-expression with full length Kidins220 **(B,** arrows). **(C)** A high magnification view of the neurite tip in (B) shows that not all Kidins220 punctae were Trio$^{1-1813}$ positive. Arrows indicate co-localising punctae, whereas arrowheads non-co-localising structures. The transfected cell and the growth cone are outlined for better visibility. **(D)** Co-expression of GFP and HA-tagged full length Kidins220 did not result in a recruitment of GFP to Kidins220-positive punctae (arrowheads). **(E)** PC12 cells were co-transfected with GFP-tagged Trio$^{1-1813}$ and HA-tagged Kidins220$^{403-1762}$ and treated as in (B). GFP-tagged Trio$^{1-1813}$ did not associate with Kidins220$^{403-1762}$-positive structures (arrowheads). **(F)** An enlargement of the neurite tip in (E) is shown. FL = full length; scale bars = 5 μm.

Figure 4: Kidins220 expression activates Rac1 but not RhoG. (A) HEK293 cells were transfected with the indicated constructs and subjected to a Rac1 activation assay as described in Supplementary materials and methods. Cells transfected with Kidins220$^{1-402}$ and to a lesser extent with full length Kidins220 showed an increase in Rac1-GTP levels. **(B)** shows the quantification of three independent experiments. Rac1-GTP levels were expressed in arbitrary units (AU), after they had been normalised to the expression of each construct and to the total Rac1 content. The activation of Rac1 by Kidins220$^{1-402}$ and full length protein is significant by the Student's t-test. **(C)** HEK293 cells were transfected with the indicated constructs and subjected to a RhoG activation assay as in (A). The first GEF domain of Trio activated endogenous RhoG, but none of the other constructs did. The average of three independent experiments is shown in **(D)**. Error bars represent s.e.m. FL = full length; p * = <0.05; p, ** = <0.01.

(E) PC12 cells were differentiated for 3 days with NGF, then fixed and stained for endogenous Kidins220 (green) and Rac1 (red). Arrows indicate overlapping punctae and arrowheads non-overlapping areas. **(F)** Trio-GFP was expressed in NGF-differentiated PC12 cells, which were subsequently fixed and immunostained for endogenous Kidins220 (blue) and Rac1 (red). Positive structures for all three proteins were observed at neurite tips (white, arrows), whereas soluble GFP was distributed rather uniformly throughout the cell **(G)**. The arrowhead indicates a Kidins220/Rac1 positive structure, which was not enriched in GFP. Scale bars = 5 μm.

Figure 5: Kidins220$^{1-402}$ overexpression inhibits NGF-dependent neurite outgrowth. **(A)** PC12 cells were transfected with GFP or the indicated HA-tagged fragments of Kidins220, differentiated with NGF for 3 days and then analysed for the length of their neurites. Neurite outgrowth was quantified by counting cells bearing neurites at least twice as long as their cell body. Quantification was obtained from three independent experiments (± s.e.m.). At least 62 cells were analysed per condition. FL = full length. **(B)** PC12 cells were co-transfected with the Raichu Rac1/Rac1-CT and HA-tagged Kidins220$^{1-402}$ (upper panel) or Kidins220$^{403-1762}$ (lower panel). The FRET ratio is shown in intensity-modulated display (IMD) format, ranging from a FRET ratio 0 to 2.5. High FRET ratios were observed inside the cell after co-transfection of Kidins220$^{1-402}$. Scale bars = 10 μm. **(C)** For quantification, the cell area (in % of the whole cell) occupied by a FRET ratio of 2.4 and above was summed up (see Materials and methods for details). These values were then compared between cells co-expressing the Raichu construct with Kidins220$^{1-402}$ (red circles) or Kidins220$^{403-1762}$ (blue squares). Each symbol represents an individual cell. The red or blue bar stands for the mean of 49 Kidins220$^{1-402}$/Raichu Rac1/Rac1-CT co-transfected cells or 42 Kidins220$^{403-1762}$/Raichu Rac1/Rac1-

CT co-transfected cells, respectively. Cells expressing Kidins220$^{1-402}$ exhibited more cell area occupied by high FRET ratios. p, * = <0.05.

Figure 6: Quantification of Trio and RhoG-induced neurite outgrowth. (A) and **(B)** PC12 E2 cells were transfected with mRFP, mRFP-CAAX or HA-tagged Kidins220 deletion mutants. After 48 hours expression in full growth medium, cells were fixed and examined for neurite outgrowth. Cells, which bore one neurite at least double the size than the diameter of its cell body, were considered to be positive (n ≥ 3 independent experiments). PC12 E2 cells were co-transfected either with GFP-tagged Trio$^{1-1813}$ **(C)** and **(D)** or RhoG **(E)** and the indicated HA-tagged Kidins220 deletion mutants or mRFP and mRFP-CAAX as negative controls. After 48 hours, double-transfected cells were examined for neurite outgrowth as previously described. Neurite outgrowth of double-transfected cells was quantified from three independent experiments. Kidins220$^{1-402}$ and the membrane-bound Kidins220$^{1-402}$-CAAX blocked Trio-induced neurite elongation **(C)** and **(D)**, whilst full length Kidins220 enhanced RhoG-induced neurite outgrowth **(E)**. Error bars represent s.e.m. At least 154 cells were analysed for each construct. FL = full length; p, ** = <0.01. **(F)** HEK293 cells were transfected with HA-tagged Kidins220$^{1-402}$, Kidins220$^{1-402}$-CAAX, mRFP or mRFP-CAAX and subjected to a membrane-cytosol fractionation. Syntaxin6 was used as membrane marker and SOD1 as marker for the cytosol. Whilst the ankyrin repeats were partially cytosolic, Kidins220$^{1-402}$-CAAX and mRFP-CAAX were associated to membrane fractions.

Figure 7: Kidins220$^{1-402}$ overexpression inhibits neurite outgrowth in hippocampal neurons. (A-C) Primary neurons were nucleofected with GFP or the indicated HA-tagged deletion mutants of Kidins220. After 1 day they were fixed and analysed for the

length of their neurites. Transfected neurons are marked with stars. **(Ab-Cb)** To detect necrotic or apoptotic cells, neurons were co-stained with propidium iodide (green) or antibodies against activated caspase 3 (red). Scale bars = 10 μm. The average of four independent experiments is shown in **(D)**. Neurons transfected with Kidins220$^{1-402}$ display impaired neurite outgrowth compared to control cells. Error bars represent s.e.m. At least 227 neurons were analysed for each construct. p, * = <0.05; p, ** = <0.01; n.s. = not significant.

Figure 8: Schematic view of the Kidins220-Trio interaction in a cellular context. **(A)** Kidins220 is a transmembrane protein and it can assist the recruitment of Trio (and/or Kalirins) to the membrane. Here, Rac1 may be activated, leading to neurite outgrowth (pathway B). At the same time, the C-terminus of Kidins220 is phosphorylated upon NGF stimulation and is involved in sustained MAPK signalling, which is also necessary for neurite outgrowth (pathway C). In parallel, Trio may translocate to the membrane with the help of RhoG (pathway A). This leads to activation of Rac1 and might explain the enhancement of neurite outgrowth when Kidins220 and RhoG are overexpressed. Trio and RhoG can bind to a variety of phospholipids (PIP_x) (Skrownek et al., 2004; Ugolev et al., 2008). **(B)** The different phenotypes generated by the expression of the ankyrin-rich Kidins220$^{1-402}$ domain and the full length protein is likely due to their different localisations. Kidins220$^{1-402}$ is distributed throughout the cell and activates Rac1, leading to an inhibition of neurite outgrowth similarly to constitutively-active Rac1 (Aoki et al., 2004). In contrast, full length Kidins220 is localised to neurite tips and is likely to determine the activation of Rac1 at these specific sites. Moreover, in full length Kidins220, the C-terminus

integrates information received from upstream signals, such as ephrins and neurotrophins, which could be transmitted to the N-terminus.

Figures

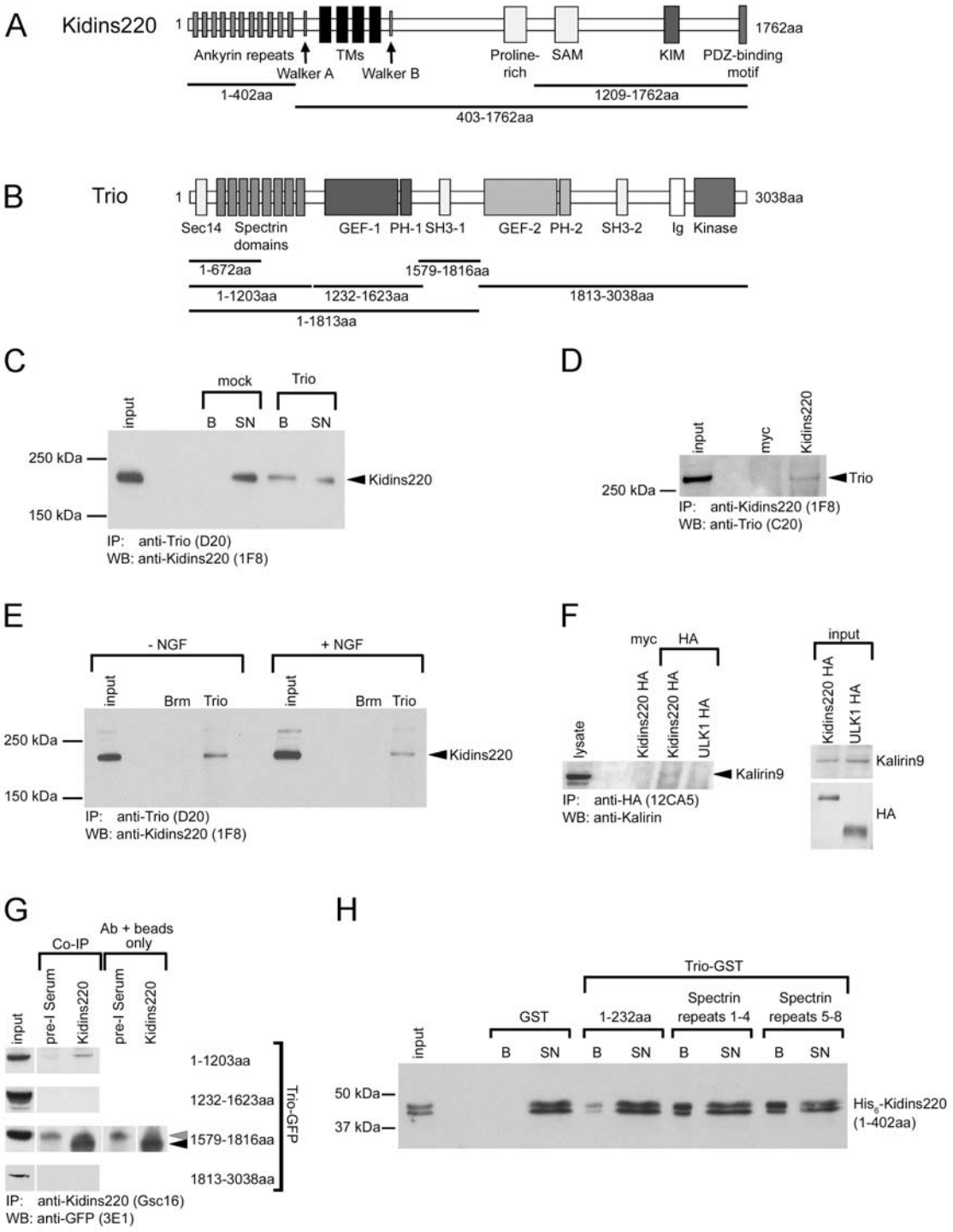

Figure 1 Neubrand et al.

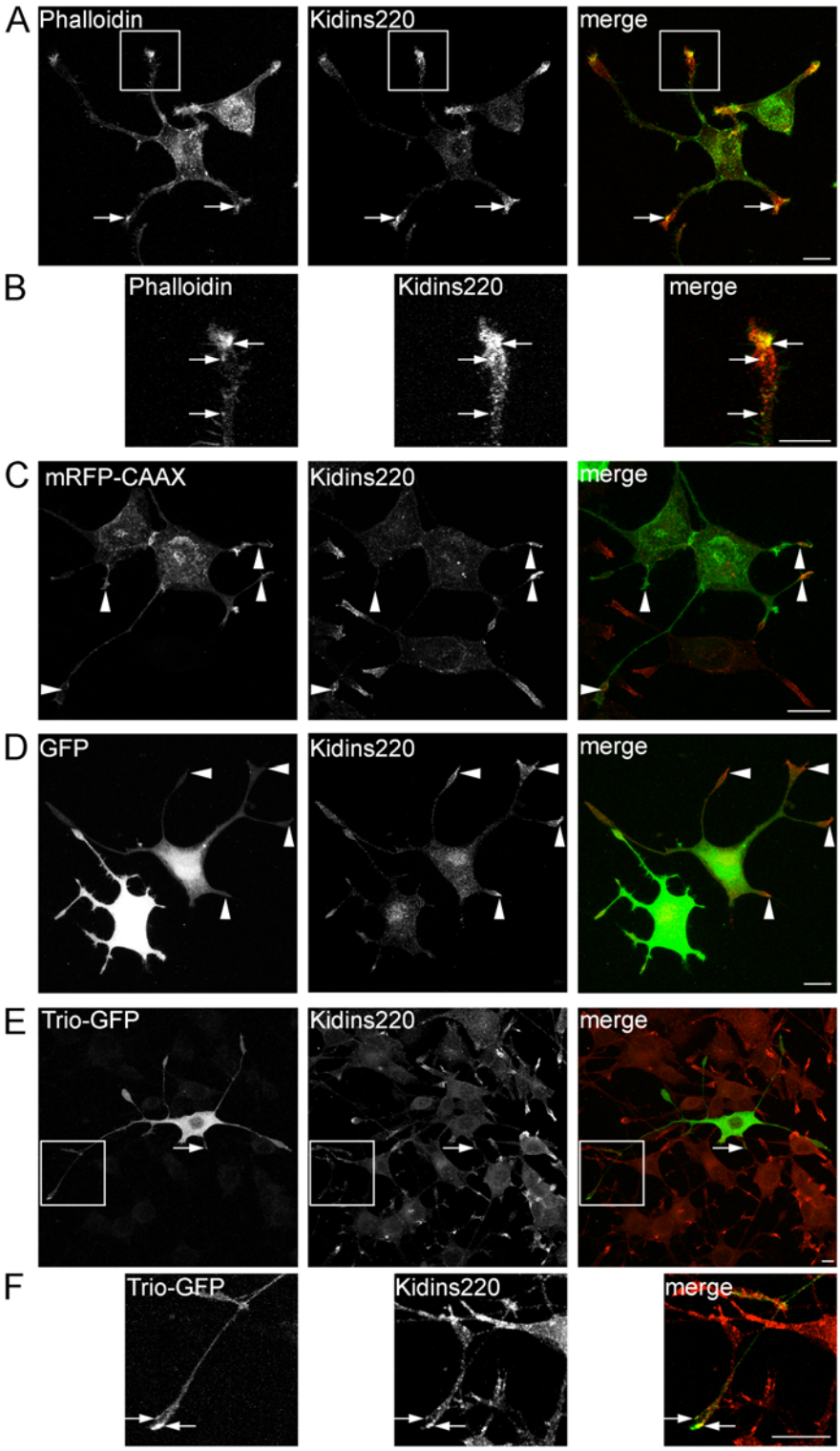

Figure 2 Neubrand et al.

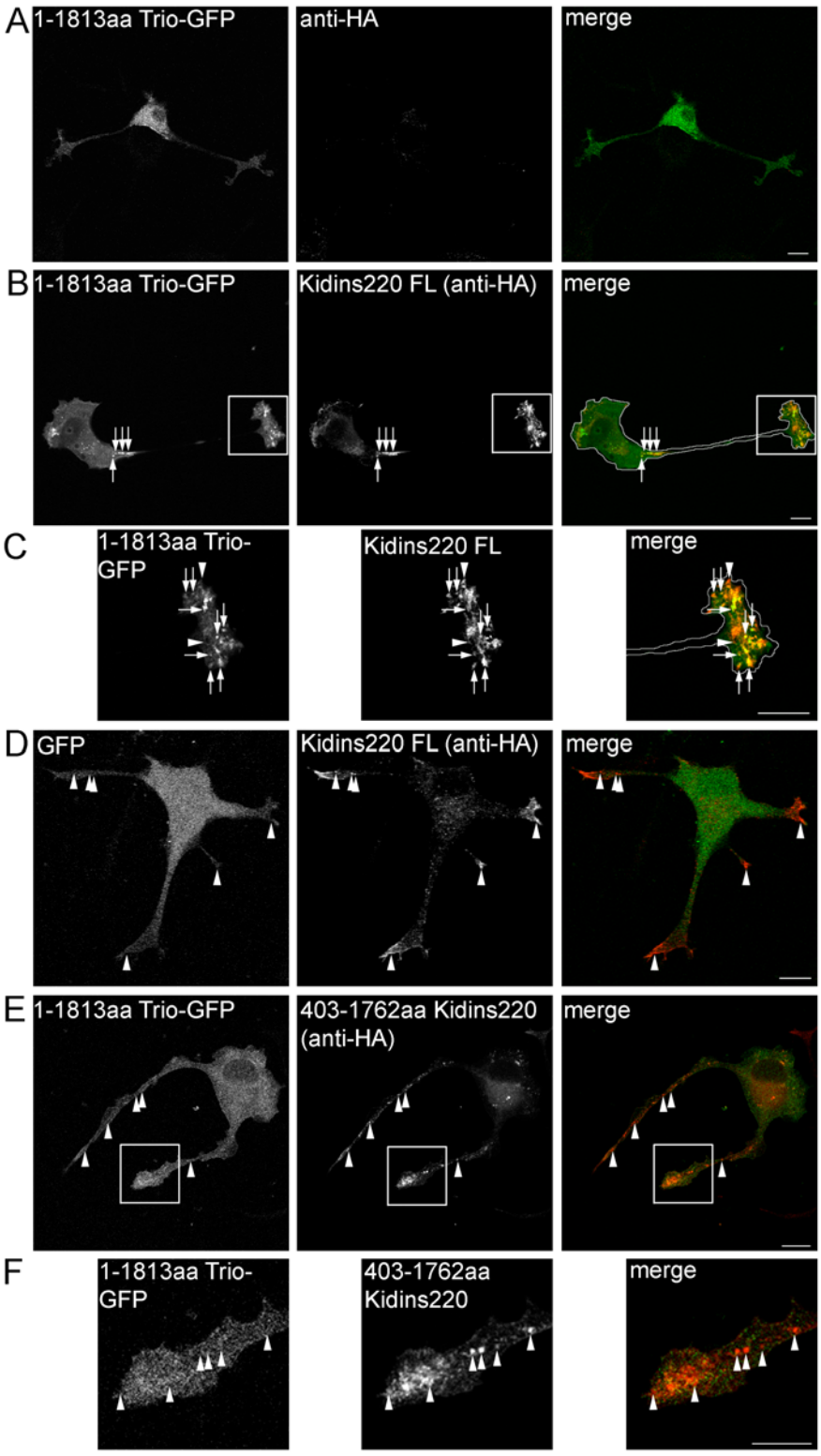

Figure 3
Neubrand et al.

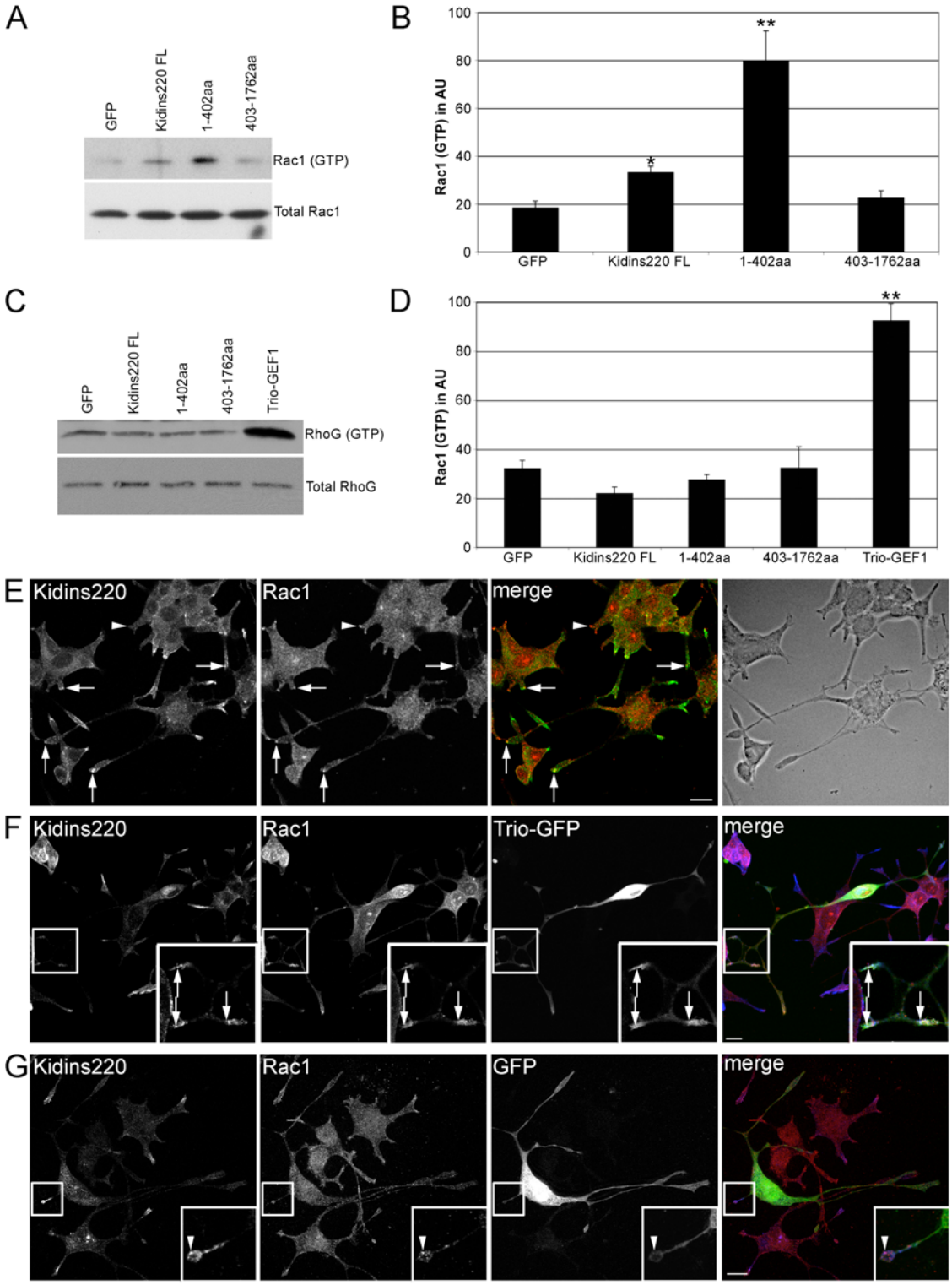

Figure 4 Neubrand et al.

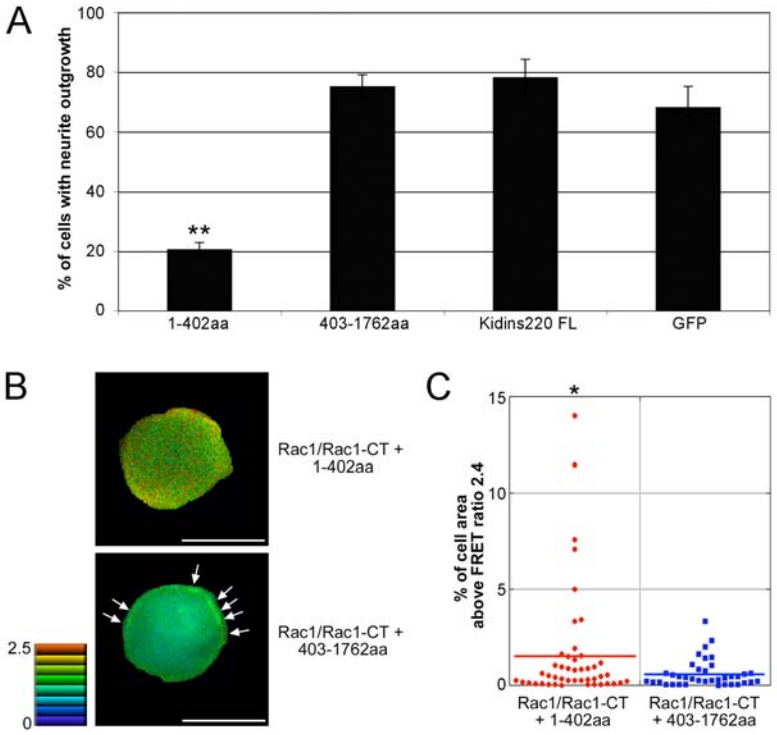

Figure 5 Neubrand et al.

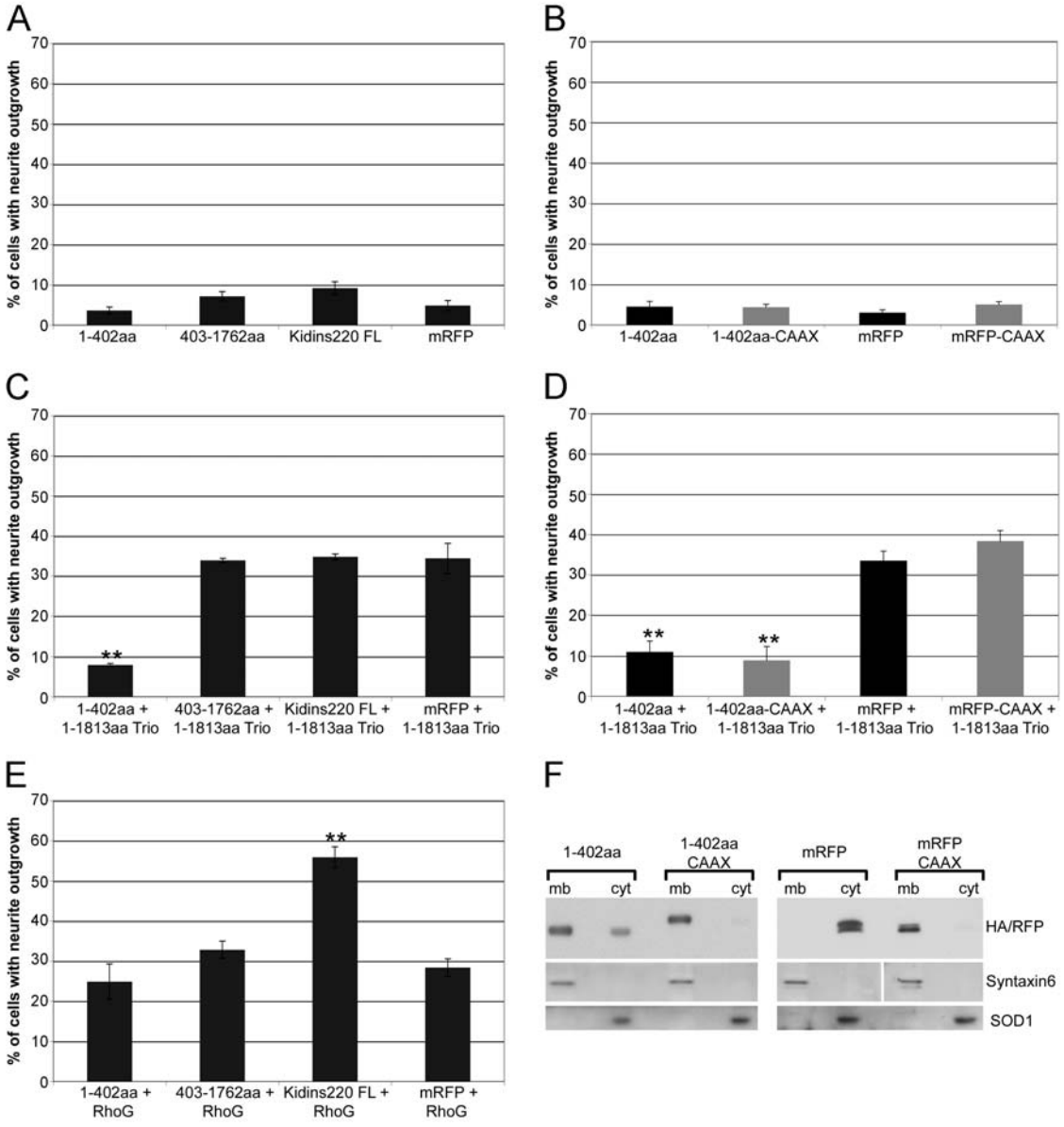

Figure 6 Neubrand et al.

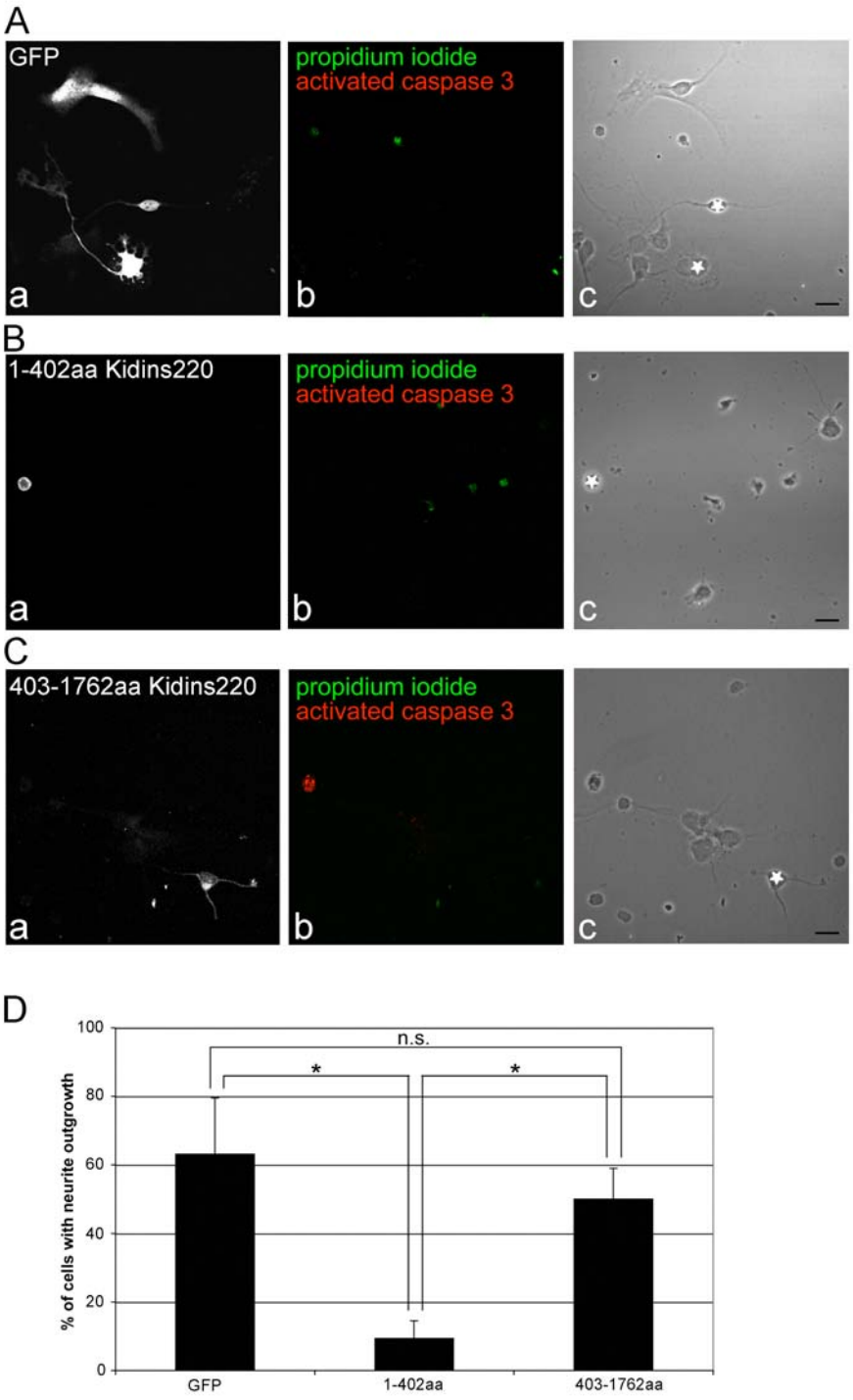

Figure 7 Neubrand et al.

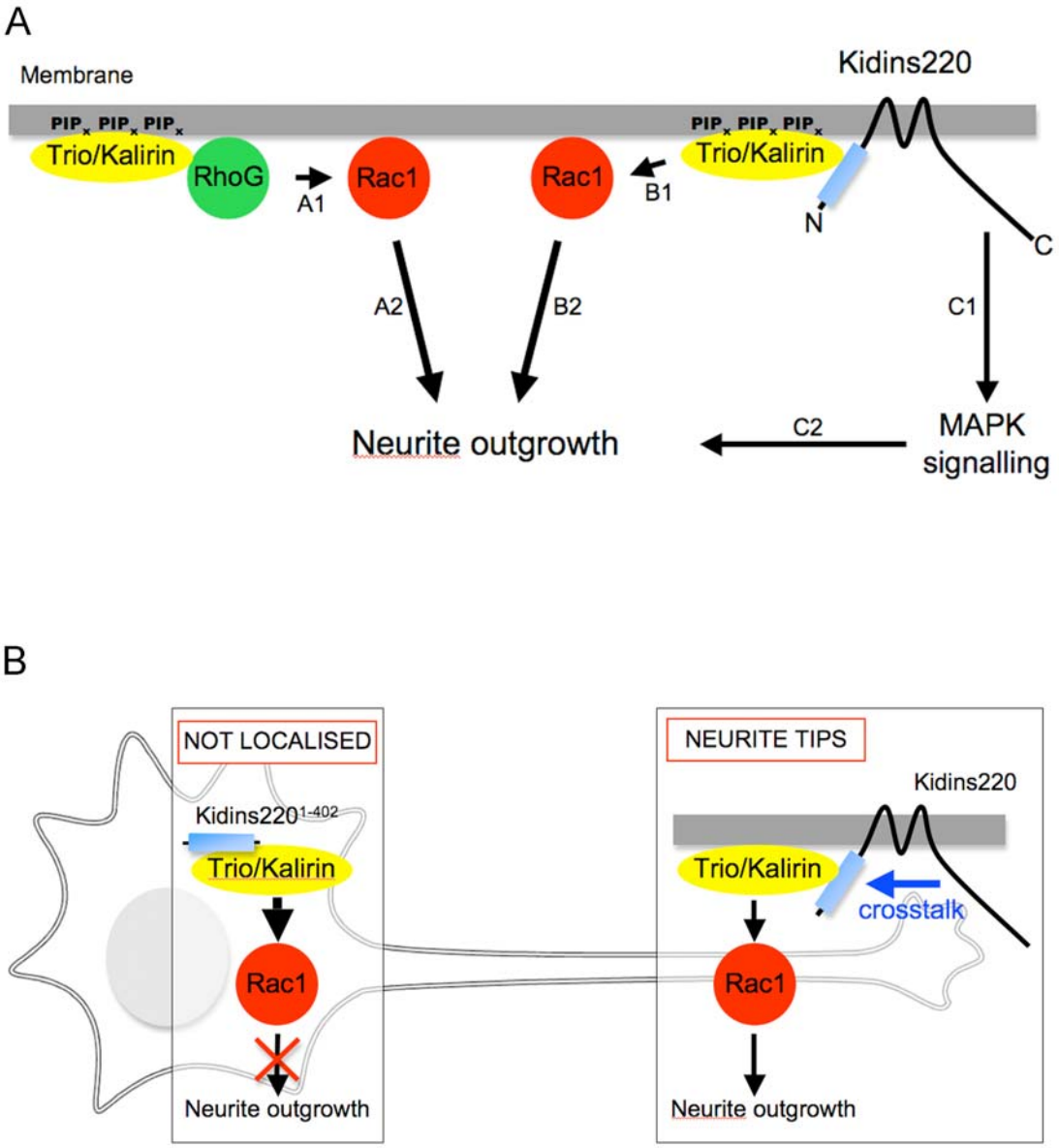

Figure 8 Neubrand et al.

Supplementary information

Materials and methods

DNA constructs. Kidins220 1-1206bp (1-402aa) and 1207-5289bp (403-1762aa) were amplified by PCR using rat full length Kidins220 cDNA (Iglesias et al., 2000) and the following primers: Kidins220$^{1-402}$ 5' primer, cat tca ccg cgg gg tca gtt ctt ata tca cag ag and 3' primer, cg cgt ggg ctt aat taa tca ttt gtt ggg tct gta gag; Kidins220$^{403-1762}$ 5' primer, c att ata ccg cgg gg gca ggc gag act ccc tac and 3' primer, gc ggg cgt taa tta aag aat gct ctc tct ctc). DNA fragments were then ligated into the PacI/SacII sites of a HA-tagged pcDNA3.1 vector (Invitrogen). GST-tagged fragments of Trio (1-232aa, 255-699aa and 696-1203aa) were subcloned from GFP-tagged Trio constructs (Estrach et al., 2002) into the EcoRI and SalI sites of pGEX4T2 (GE Biotech). Constructs used in the yeast two-hybrid analysis were subcloned into the NdeI/NotI sites of pGBKT7 (bait), or the EcoRI/XhoI sites of pGADT7 (prey), both from Clontech. For the preparation of Kidins220$^{1-402}$-CAAX, the stop codon in HA-Kidins220$^{1-402}$ was first deleted by site-directed mutagenesis (TGA to TCG), using the 5' primer tac aga ccc aac aaa tcg tta att aat tcg aat c and the 3' primer gat tcg aat taa tta acg att tgt tgg gtc tgt a. The CAAX box of the mRFP-CAAX plasmid (a kind gift of S. Hooper and E. Sahai (Gaggioli et al., 2007)), was amplified by PCR with the 5' primer cgc gcc tta att aac aag atg agc aag gac and the 3' primer cgc gcc gca tcg att tac ata att aca cac ttt g, digested with PacI and ClaI and ligated at the 3' of the modified HA-Kidins220$^{1-402}$ plasmid. All clones were verified by DNA sequencing.

Antibodies and immunostaining. Fixation, immunofluorescence staining and image acquisition were performed as previously described (Bracale et al., 2007). In Fig. 2,

cells are shown as projections of confocal stacks, whereas in Figs 3, 4 individual confocal stacks are presented.

The following primary antibodies were used: mouse anti-Kidins220 (Bracale et al., 2007), rabbit anti-Kidins220 (Iglesias et al., 2000), goat anti-Trio C20 and D20 (Santa Cruz), mouse anti-Rac1 (clone 102/Rac1, BD Biosciences) and mouse anti-Rac1 (clone 23A8, Millipore), mouse anti-RhoG (clone 1F3B3E5, Santa Cruz), rabbit anti-GST (GE Biotech), mouse anti-α-tubulin (clone B512, Sigma), rat anti-HA (clone 3F10, Roche), mouse anti-HA (clone 12CA5, CRUK), rabbit anti-RFP (Abcam), rabbit anti-Syntaxin6 (STO112, CRUK), rabbit anti-SOD1 (Abcam), rabbit anti-Kalirin (US Biological), mouse anti-GFP (clone 3E1, CRUK), rabbit anti-activated caspase 3 (RD Systems), mouse anti-myc (clone 9E10, CRUK), goat anti-Brm (Santa Cruz) and mouse anti-RGS-His_6 (Qiagen) antibodies. AlexaFuor488-, 546- and 647-conjugated secondary antibodies were from Molecular Probes.

His_6-tagged Kidins220 protein purification. Kidins220 1-402aa DNA fragment was inserted into a M15pQE31 vector (Qiagen) to generate a His_6-tagged fusion protein. Protein expression was induced with 0.4 mM IPTG. Bacteria were grown for additional 3.5 h at 25°C, pelleted, resuspended in 25 mM Tris-HCl pH 7.8, 300 mM KCl, 2 mM 2-mercaptoethanol and protease inhibitors and lysed using the French Press. After centrifugation, the pellet was resuspended in 8 M urea in PBS containing 0.05 % Tween and after removal of cell debris, the supernatant was incubated with Ni-NTA agarose (Qiagen) at 25°C for 45 min. Beads were washed initially with 100 mM Tris-HCl pH 8.0, 6 M urea, 20 mM imidazole, following by a gradient in which the concentration of urea was slowly brought to 0. The His_6-tagged protein was eluted with 500 mM imidazole and dialyzed against 20 mM HEPES-NaOH pH 7.4, 150 mM NaCl, 0.1 M

urea and 5 % glycerol.

Western Blotting and Immunoprecipitation. For immunoprecipitation, PC12 cells were lysed with IP buffer (10 mM Tris-HCl pH 8.0, 150 mM NaCl, 1% Nonidet-P40, 1 mM EDTA and protease inhibitors (Roche)). Lysates (1 mg per sample) were precleared with protein G sepharose (GE Biotech), centrifuged at 15,000 g and the supernatant was incubated for 3 hours with 10 μg of anti-Trio D20 or anti-Kidins220 (Gsc16 or 1F8) antibodies. A mouse anti-myc antibody, a goat anti-Brm antibody, a rabbit-pre-immune serum or no antibody (mock) was included as negative control, depending on the species of the immunoprecipitating antibody. Immunocomplexes were recovered with protein G sepharose overnight, washed with PBS and 0.1% Nonidet-P40 (supplemented with 500 mM NaCl for Fig. 1E,F), and then prepared for SDS-PAGE. Horseradish peroxidase-conjugated secondary antibodies (DakoCytomation) and ECL (GE Biotech) were used for detection.

GST protein purification and direct binding assay. GST fusion proteins corresponding to different Trio fragments were expressed in *E. coli* BL21 (DE3) cells. 1 l of log phase cells was induced with 1 mM IPTG and shaken at 22°C overnight. Bacteria were lysed in 20 ml of lysis buffer (20 mM Tris-HCl pH 7.5, 0.1% Triton X-100, 1 μg/ml lysozyme, 1 μg/ml DNAse), sonicated, and centrifuged at 138,000 g at 4°C for 20 minutes. The clarified lysate was mixed at 4°C for 1 hour with glutathione-sepharose 4B (GE Biotech) equilibrated with 20 mM Tris-HCl pH 7.5, 0.1% Triton X-100. Beads were washed 4 times with this buffer, once with 50 mM Tris-HCl pH 8.0, and then used in the binding assay.

The binding of His_6-tagged Kidins220$^{1-402}$ to various GST fusion proteins was assayed in binding buffer (25 mM HEPES-NaOH pH 7.2, 125 mM KOAc, 2.5 mM MgOAc, 1 mM 2-mercaptoethanol, 0.1% Triton X-100) as described previously (Neubrand et al., 2005), using 30 μg of the purified GST fusion proteins and 16.6 μg/ml of His_6-tagged Kidins220$^{1-402}$ in 0.9 ml. Briefly, samples were incubated for 1 hour at 4°C and beads were recovered by centrifugation. After 4 washes with binding buffer, 1/10th of each pellet and 1/60th of each supernatant were subjected to SDS-PAGE and Western blotting. Blots were probed with anti-His_6 antibodies (Qiagen), and detected by ECL.

RhoGTPase activation assays. For the Rac1 activation assay, a GST-pulldown using the CRIB domain of Pak1 was performed (Briancon-Marjollet et al., 2008). *E. coli* B21 bacteria transformed with a pGEX-vector encoding GST-CRIB were grown at 37°C until they reached an OD_{600} of 0.6. Protein expression was induced by IPTG (0.1 mM final concentration) and cultures were further incubated for 3 h at 20°C. Bacteria were harvested by centrifugation at 6,000 g for 15 min at 4°C, resuspended in breaking buffer (20 mM Hepes-NaOH pH 7.5, 120 mM NaCl, 2 mM EDTA, 10 % glycerol, 100 mM PMSF) and sonicated 3 times for 1 min at 35 % intensity. After centrifugation at 10,000 rpm for 20 min, Nonidet-P40 (0.5 % final concentration) was added and the lysate was incubated with glutathione-sepharose beads for 30 min at 4°C. Beads were washed in lysis buffer (25 mM Hepes-NaOH pH 7.5, 1 % Nonidet-P40, 10 mM $MgCl_2$, 100 mM NaCl, 5 % glycerol, 100 mM PMSF, phosphatase inhibitors) and in binding buffer (25 mM Hepes-NaOH pH 7.5, 0.5 % Nonidet-P40, 30 mM $MgCl_2$, 40 mM NaCl, 1 mM dithiothreitol (DTT)). HEK293 cells were transfected with the indicated constructs and scraped with ice-cold lysis buffer. Lysates were centrifuged for 30 s at 14,000 rpm, the supernatant incubated with 20 μg GST-CRIB beads for 30 min at 4°C and washed with

binding buffer. Finally, beads were resuspended in 20 µl of sample buffer and half of it was loaded on an SDS-PAGE together with 15 µl of the lysate to determine the total amount of Rac1 per sample. Nitrocellulose membranes were revealed by an anti-Rac1 antibody.

For the RhoG activation assay, a plasmid encoding the GST-tagged RhoG-binding domain of kinectin (KID1) (Vignal et al., 2001) was transformed into *E. coli* BL21. Protein expression was induced with 0.1 mM IPTG and bacteria were further incubated at for 3 h at 25°C, prior to centrifugation at 4,000 rpm for 15 min and resuspension in PBS supplemented with 1 mM DTT, 100 µM PMSF and 1 µg/ml lysozyme. The lysate was incubated for 30 min on ice and subsequently 0.1 % Triton X-100, 10 mM $MgCl_2$ and 0.1 µg/ml DNAse (final concentrations) were added. After 30 min on ice, the lysate was centrifuged for 25 min at 138,000 g. The supernatant was incubated with glutathione-sepharose beads pre-equilibrated in PBS, 10 mM DTT, 1 % Triton X-100. Pellets were washed with PBS, 10 mM DTT, 1 % Triton X-100 and at least 20 µg GST-KID1 was subjected to GST-pull-down per condition. The pull-down was performed as described for the Rac1 activation assay using a lysis buffer containing 50 mM Tris-HCl pH 7.5, 125 mM NaCl, 5 mM $MgCl_2$, 1 % Triton X-100, 0.5 % sodium deoxycholate, 0.1 % SDS, 1 mM DTT and protease inhibitors, and a binding buffer containing 50 mM Tris-HCl pH 7.5, 125 mM NaCl, 5 mM $MgCl_2$, 1 % Triton X-100 and protease inhibitors. Finally, beads were resuspended in 20 µl SDS sample buffer and loaded on an SDS-PAGE together with 15 µl of the lysate to determine the total RhoG amount per sample. PVDF membranes were revealed with an anti-RhoG antibody.

Membrane-cytosol fractionation. HEK293 cells transfected with the indicated constructs were scraped into homogenisation buffer (20 mM Hepes-KOH pH 7.2, 2 mM

EDTA, 150 mM KCl, supplemented with Roche Complete protease and phosphatase inhibitors), then lysed by passing the cells through a 27G needle. Cell lysates were centrifuged at 4500 rpm for 5 min at 4°C to pellet unbroken cells and nuclei. The postnuclear supernatant was centrifuged at 100000 g (45000 rpm, TLA45 rotor) for 1 h at 4°C. Membrane pellets were resuspended in RIPA buffer (50 mM Tris-HCl pH 7.2, 150 mM NaCl, 5 % Triton X-100, 1 % deoxycholate, 0.1 % SDS). Finally, 1/50th of membrane and cytosol fractions were loaded on an SDS-PAGE. PVDF membranes were probed with anti-syntaxin6 antibodies as a marker for the membrane fraction and with anti-SOD1 antibodies for the cytosol.

References

Bracale, A., Cesca, F., Neubrand, V. E., Newsome, T. P., Way, M. and Schiavo, G. (2007). Kidins220/ARMS is transported by a kinesin-1-based mechanism likely to be involved in neuronal differentiation. *Mol Biol Cell* **18**, 142-52.

Briancon-Marjollet, A., Ghogha, A., Nawabi, H., Triki, I., Auziol, C., Fromont, S., Piche, C., Enslen, H., Chebli, K., Cloutier, J. F. et al. (2008). Trio mediates netrin-1-induced Rac1 activation in axon outgrowth and guidance. *Mol Cell Biol* **28**, 2314-23.

Estrach, S., Schmidt, S., Diriong, S., Penna, A., Blangy, A., Fort, P. and Debant, A. (2002). The Human Rho-GEF trio and its target GTPase RhoG are involved in the NGF pathway, leading to neurite outgrowth. *Curr Biol* **12**, 307-12.

Gaggioli, C., Hooper, S., Hidalgo-Carcedo, C., Grosse, R., Marshall, J. F., Harrington, K. and Sahai, E. (2007). Fibroblast-led collective invasion of carcinoma cells with differing roles for RhoGTPases in leading and following cells. *Nat Cell Biol* **9**, 1392-400.

Iglesias, T., Cabrera-Poch, N., Mitchell, M. P., Naven, T. J., Rozengurt, E. and Schiavo, G. (2000). Identification and cloning of Kidins220, a novel neuronal substrate of protein kinase D. *J Biol Chem* **275**, 40048-56.

Neubrand, V. E., Will, R. D., Mobius, W., Poustka, A., Wiemann, S., Schu, P., Dotti, C. G., Pepperkok, R. and Simpson, J. C. (2005). Gamma-BAR, a novel AP-1-interacting protein involved in post-Golgi trafficking. *Embo J* **24**, 1122-33.

Vignal, E., Blangy, A., Martin, M., Gauthier-Rouviere, C. and Fort, P. (2001). Kinectin is a key effector of RhoG microtubule-dependent cellular activity. *Mol Cell Biol* **21**, 8022-34.

Supplementary figure legends

Supplementary Table 1: Confirmed positive hits of the yeast-two hybrid screen. This table summarises the positive clones obtained by screening a rat brain cDNA library using the N-terminal fragment of Kidins220 (Kidins220$^{1-402}$) in the AH109 yeast reporter strain.

Supplementary Figure 1: Interaction between Kidins220 and Trio. (A) A yeast-two-hybrid screen revealed an interaction between Kidins220 and Trio. To verify this binding, Kidins220$^{1-402}$ and Kidins220$^{1209-1762}$ were co-transformed with Trio$^{1-672}$. Only co-transformation of the N-termini of both proteins resulted in yeast growth. **(B)** To map the Kidins220 binding domains on Trio, PC12 cells were transfected with GFP-tagged Trio deletion mutants and co-immunoprecipitations were performed with anti-Kidins220 antibodies. Immunoglobulin contaminating bands of the anti-Kidins220 antibodies and of the pre-immune serum (Pre-I) are indicated with black and grey arrowheads, respectively. Only Trio$^{1-1203}$ could be immunoprecipitated with Kidins220

antibodies. **(C)** The nitrocellulose membrane of the experiment in Fig. 1H was stained with Ponceau Red before incubation with anti-His_6 antibodies. SN = supernatant; B = beads.

Supplementary Figure 2: Rac1 activation by Kidins220. (A) HEK293 cells were transfected with the indicated constructs and their expression levels tested by Western Blot using anti-HA and anti-GFP antibodies. Cell lysates were then subjected to the Rac1 activation assay shown in Fig. 4A. **(B)** The nitrocellulose membrane of the experiment in Figure 4A was stained with Ponceau Red before incubation with anti-Rac1 antibodies. **(C)** HEK293 cells were transfected with the indicated constructs and their expression levels tested by Western Blot using anti-HA and anti-GFP antibodies. Cell lysates were then subjected to the RhoG activation assay in Fig. 4C. **(D)** The PVDF membrane of the experiment in Fig. 4C was stained with Ponceau Red prior to anti-RhoG antibody incubation.

Supplementary Figure 3: Effect of Kidins220 deletion mutants on NGF-induced neurite outgrowth in PC12 cells. (A) and **(B)** PC12 cells were transfected with GFP or the indicated HA-tagged fragments of Kidins220, differentiated with NGF for 3 days and analyzed for neurite outgrowth. Note the ubiquitous distribution of $Kidins220^{1-402}$ (inset). In **(B),** representative cells were imaged using the same settings and images converted into pseudocolours using Metamorph to compare their expression levels. Low expression is indicated in violet and strong expression in white. Low $Kidins220^{1-402}$ expression was found throughout the cell, whereas high expression of $Kidins220^{403-1762}$ and full length Kidins220 were observed at the neurite tips. (A) and (B) represent examples for cells quantified in Fig. 5A. Transfected cells are marked with stars. FL =

full length; scale bars = 10 μm. **(C)** PC12 cells were treated as in (A) and (B) and then subjected to Western Blotting to analyse the overall expression levels of the different HA-tagged Kidins220 constructs. Kidins220$^{1-402}$ is weakly expressed compared to Kidins220$^{403-1762}$ and full length Kidins220.

Supplementary Figure 4: Effect of Kidins220 deletion mutants on Trio-induced neurite outgrowth. PC12 E2 cells were co-transfected with GFP-Trio$^{1-1813}$ and the indicated HA-tagged Kidins220 deletion mutants, or mRFP or mRFP-CAAX as negative control. After 48 hours, cells were fixed and double-transfected cells examined for neurite outgrowth as previously. This figure represents examples of cells quantified in Fig. 6C and D. Transfected cells are marked with stars. FL = full length; scale bars = 10 μm.

Supplementary Figure 5: Effect of Kidins220 deletion mutants on neurite outgrowth in PC12 E2 cells. PC12 E2 cells were transfected with mRFP, mRFP CAAX or the indicated HA-tagged deletion mutants of Kidins220. After 48 hours, cells were fixed and examined for neurite outgrowth. Similarly to Kidins220$^{1-402}$, Kidins220$^{1-402}$-CAAX is ubiquitously distributed throughout the cell (inset). This figure shows examples of cells quantified in Fig. 6A and 6B. Transfected cells are marked with stars. FL = full length; scale bars = 10 μm.

Supplementary Figure 6: Effect of Kidins220 deletion mutants on RhoG-induced neurite outgrowth. PC12 E2 cells were co-transfected with wild type RhoG-GFP and the indicated HA-tagged Kidins220 deletion mutants or mRFP. 48 hours later, cells were immunostained and analyzed for neurite outgrowth. This figure represents

examples of cells quantified in Fig. 6E. Transfected cells are marked with stars. FL = full length; scale bars = 10 μm.

Supplementary figures

Protein description	**Protein ID**
Aldehyde reductase	BAA01627.1
ANKRD27	BAB70755.1
APC subunit 2	AAF05751.1
ATPase inhibitor protein	BAA02424.1
Ca^{2+}/calmodulin-dependent kinase II	AAA41866.1
Dynamin I	CAA38397.1
Erbin	AAF77047.1
Hic5 / TGF-β 1 induced transcript 1	AAK01175.1 / AAH02049.1
Homolog to small nuclear ribonucleoprotein F	BAB25551.1
Mitochondrial ribosomal protein S15	BAB41000.1
(Na^+, K^+)-ATPase-β-2 subunit	AAA40782.1
Non-neuronal enolase	CAA26456.1
Syne-1	AAG24393.1
Trio	AAC34245.1
Zygin I	AAC71216.2

Supplementary Table 1 Neubrand et al.

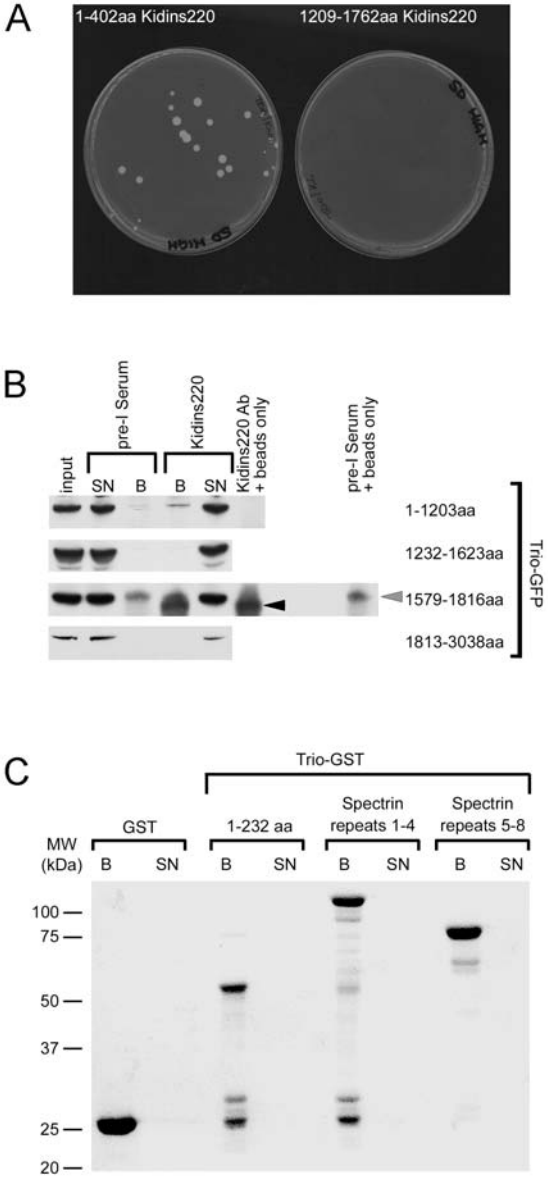

Supplementary Figure 1 Neubrand et al.

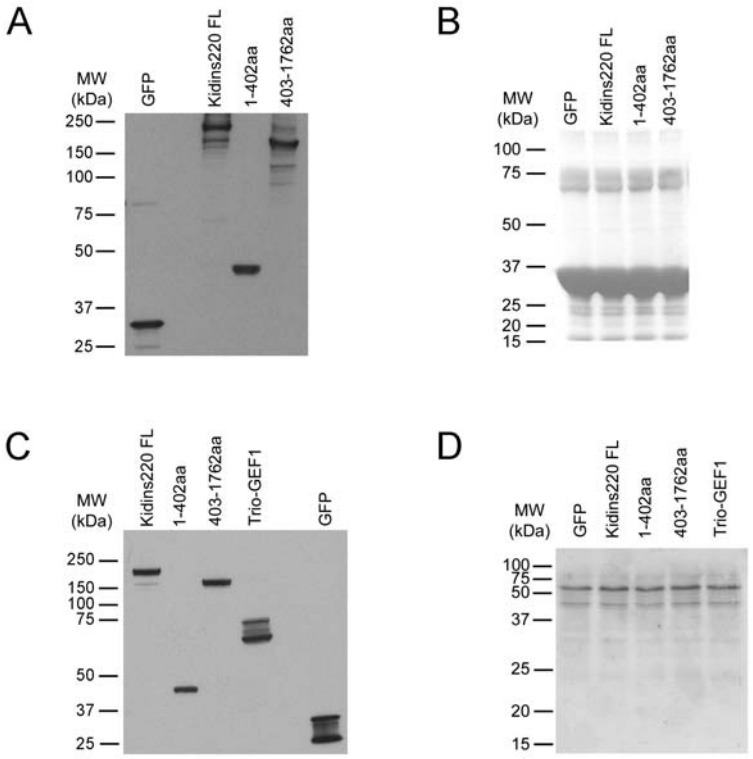

Supplementary Figure 2 Neubrand et al.

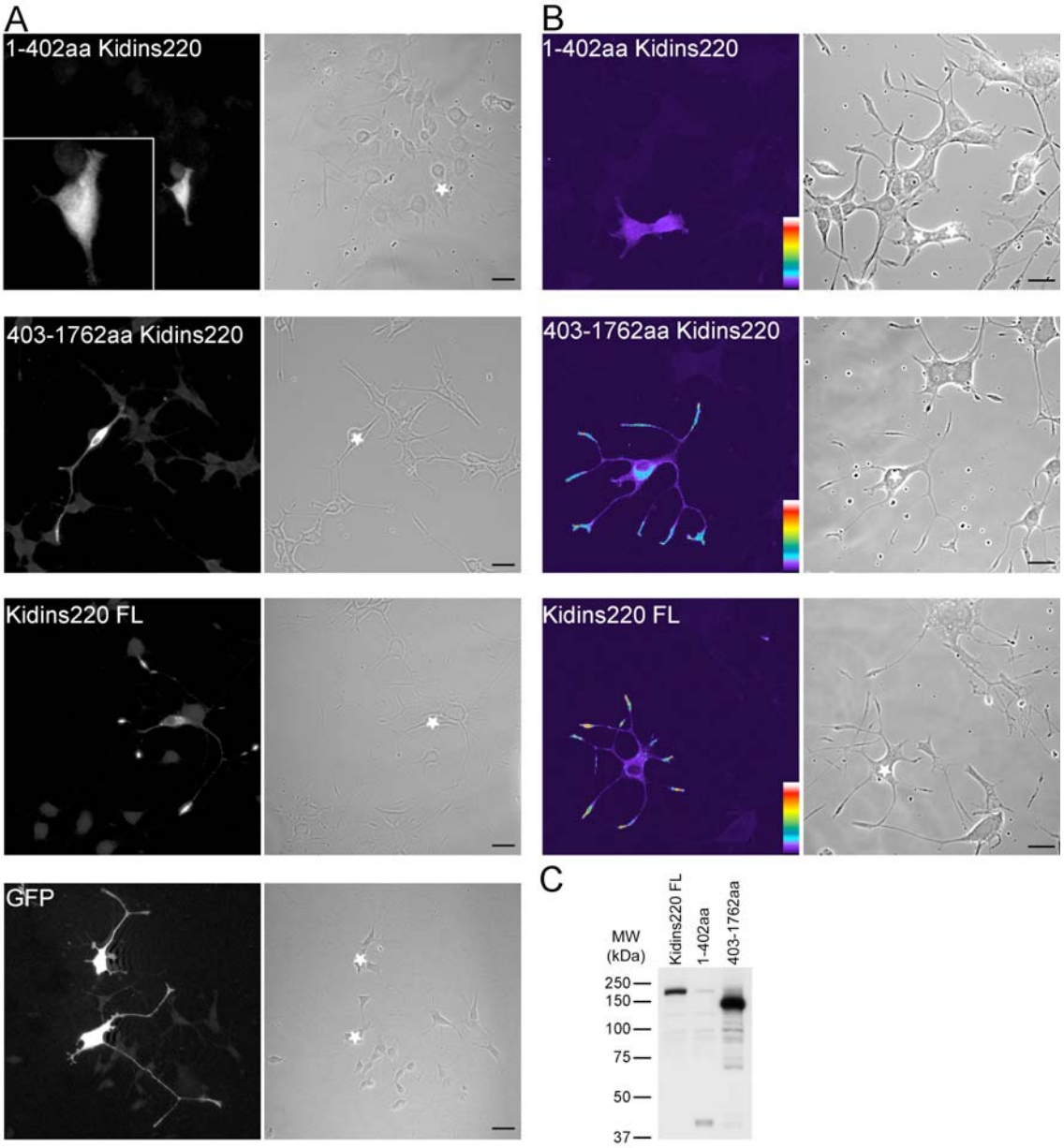

Supplementary Figure 3 Neubrand et al.

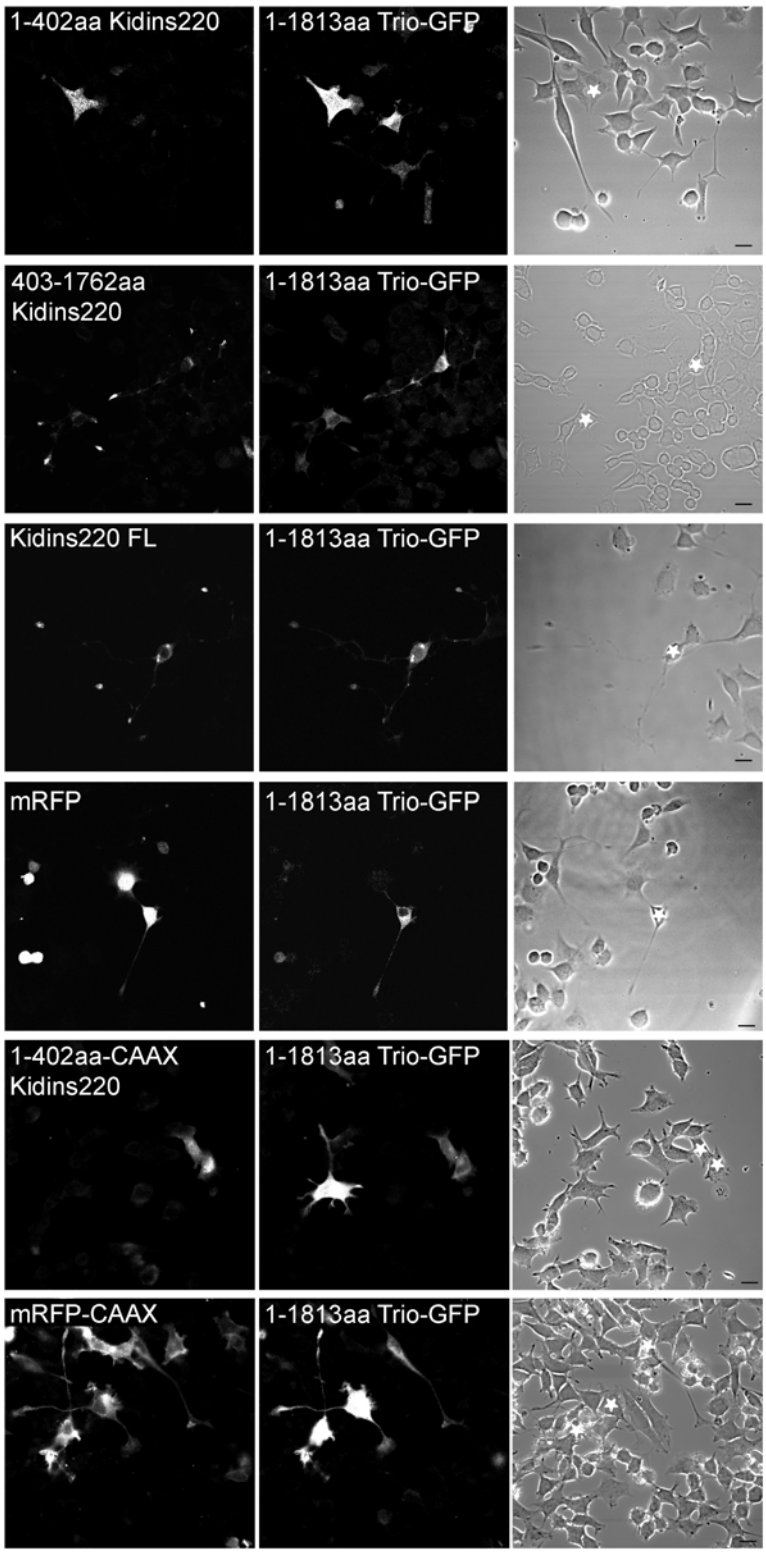

Supplementary Figure 4
Neubrand et al.

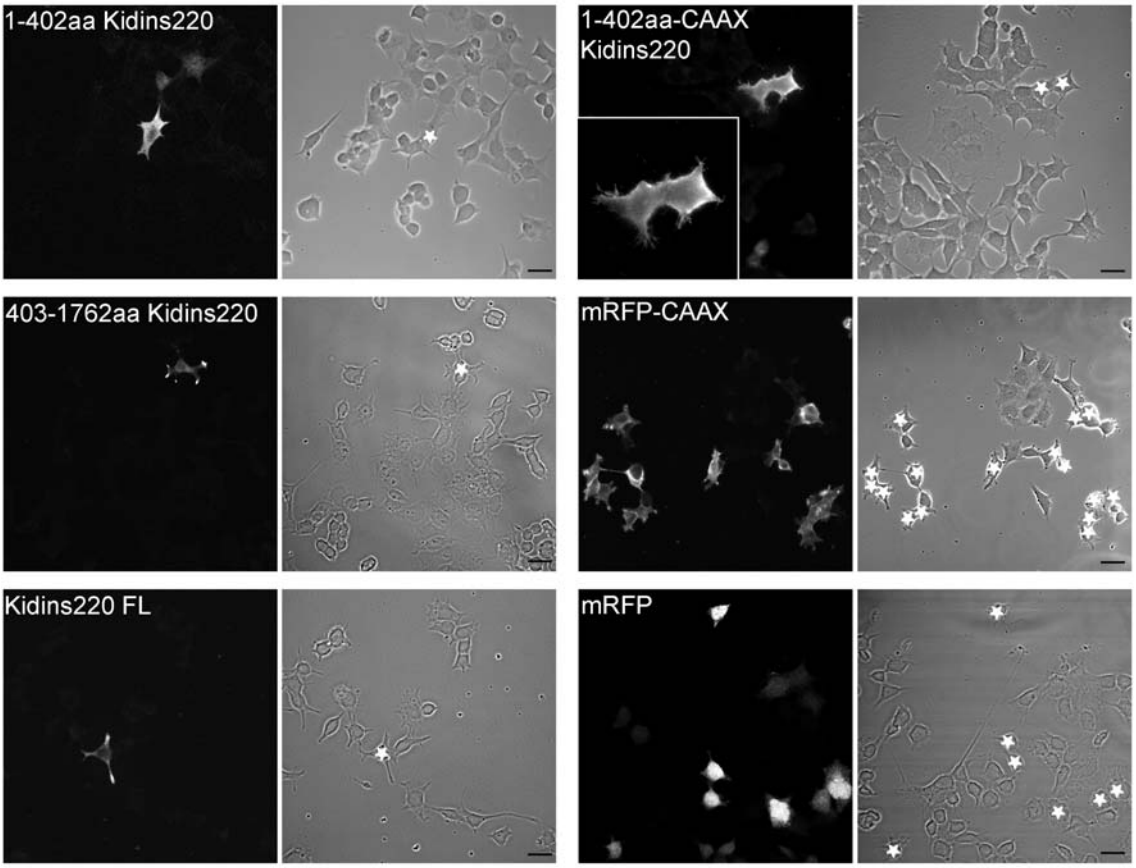

Supplementary Figure 5 Neubrand et al.

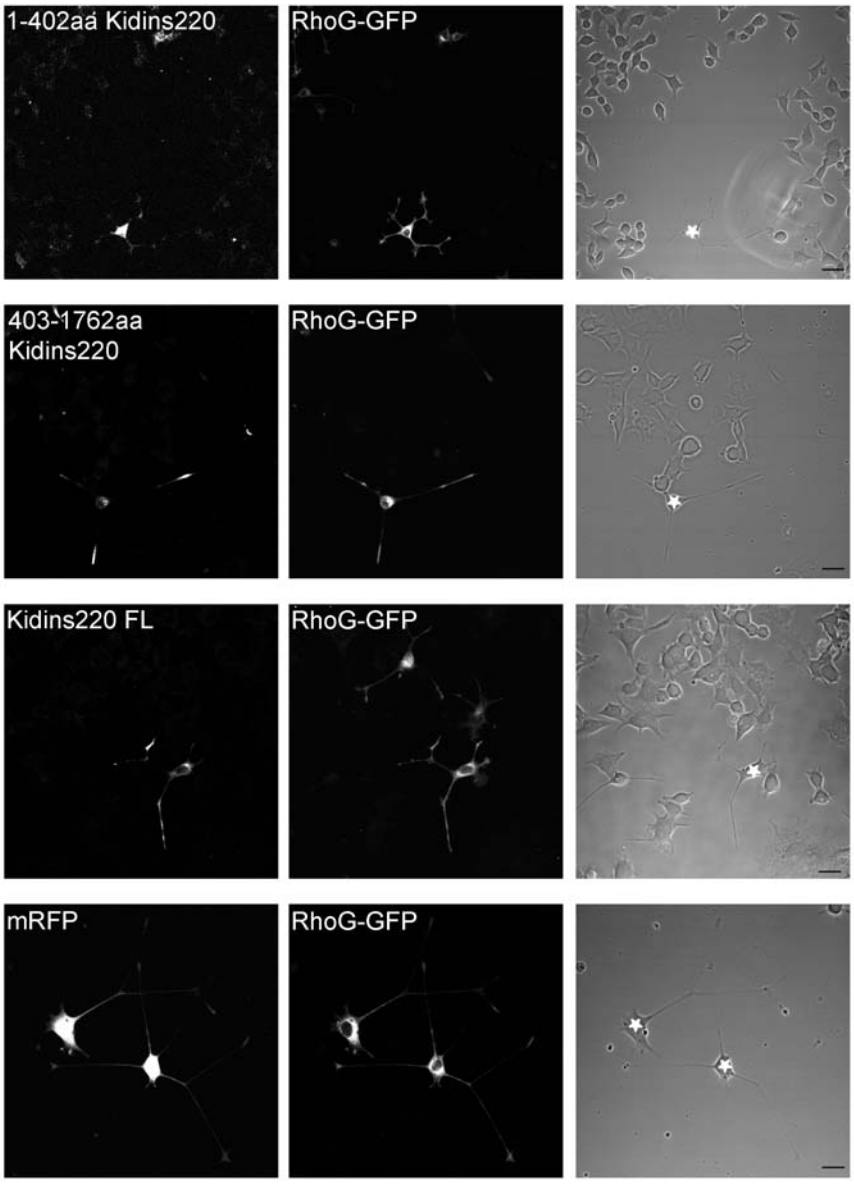

Supplementary Figure 6 Neubrand et al.